Title: **A frequency-dependent mobilization of heterogeneous pools of synaptic vesicles shapes presynaptic plasticity**

Frédéric Doussau[1], Hartmut Schmidt[2], Kevin Dorgans[1], Antoine M. Valera[1,3], Bernard Poulain[1], and Philippe Isope[1].

[1]Institut des Neurosciences Cellulaires et Intégratives, CNRS UPR 3212, Université de Strasbourg, 67084 Strasbourg, France

[2]Carl-Ludwig Institute for Physiology, University of Leipzig, 04103 Leipzig, Germany

[3]Present Address: Department of Neuroscience, Physiology and Pharmacology, University College London, London WC1E 6BT

Corresponding author: Frédéric Doussau
INCI, CNRS UPR 3212
5, rue Blaise Pascal
67084 Strasbourg, France
E-mail: doussau@inci-cnrs.unistra.fr

Number of pages: 30
Number of figures: 8

The authors declare no competing financial interests

A frequency-dependent mobilization of heterogeneous pools of synaptic vesicles shapes presynaptic plasticity

F. Doussau, H. Schmidt, K. Dorgans, A. M. Valera, B. Poulain and P. Isope.

ABSTRACT

The segregation of the readily releasable pool of synaptic vesicles (RRP) in sub-pool which are differentially poised for exocytosis shapes short-term plasticity at depressing synapses. Here, we used in vitro recording and modeling of synaptic activity at the facilitating mice cerebellar granule cell to Purkinje cell synapse to demonstrate the existence of two sub-pools of vesicles in the RRP that can be differentially recruited upon fast changes in the stimulation frequency. We show that upon low-frequency stimulation, a population of fully-releasable vesicles is silenced, leading to full blockage of synaptic transmission. A second population of vesicles, reluctant to release by simple stimuli, is recruited in a millisecond time scale by high-frequency stimulation to support an ultrafast recovery of neurotransmitter release after low-frequency depression. The frequency-dependent mobilization or silencing of sub-pools of vesicles in granule cell terminals should play a major role in the filtering of sensorimotor information in the cerebellum.

INTRODUCTION

In neural networks, transfer of information largely relies on the ability of presynaptic terminals to transduce information encoded by changes in action potentials (APs) firing rate into changes in the release of neurotransmitters. During trains of APs, the immediate tuning of synaptic efficacy is determined by the combination of multiple parameters including AP frequency, past firing activities, number of release-competent synaptic vesicles (SVs), also referred as the readily-releasable pool (RRP), probability of

28   release (p_r), or the number of release sites (N). To date, the deciphering of cellular

29   mechanisms underlying synaptic efficacy is challenged by a non-unified view of the

30   identity of SVs belonging to the RRP (Neher, 2015). Depending on studies, the RRP

31   may correspond to a large population of docked SVs releasable by hyperosmotic

32   stimulation or at the opposite is restricted to SVs releasable by a single AP (Moulder and

33   Mennerick, 2005; Pan and Zucker, 2009; Neher, 2015). Besides, there is increasing

34   evidence showing that the RRP is constituted with heterogeneous population of SVs

35   differentially poised for exocytosis and sequentially recruited before the fusion step. In

36   the calyx of Held, the RRP can be separated into a fast-releasing pool (FRP) and a

37   slowly releasing one (SRP) (Sakaba and Neher, 2001; Sakaba, 2006; Schneggenburger

38   et al., 2012) and during a train of APs, SRP are first converted to the FRP and then

39   maturate to a superpriming step before acquiring a high release rate (Lee et al., 2012,

40   2013). In the cerebellar cortex, at GC-molecular layer interneuron (MLI), a segregation of

41   the RRP in two pools mobilized in a two-step process has also been described while

42   with faster kinetics for the transition between the two steps (Ishiyama et al., 2014; Miki et

43   al., 2016). Finally, these studies draw a model in which synaptic plasticity during high-

44   frequency trains is shaped by the kinetics of mobilization of sub-pools of SVs in the RRP

45   (Pan and Zucker, 2009; Miki et al., 2016). However, the way synapses manage these

46   pools/steps upon a broad bandwidth of stimulation frequency are still unknown.

47   Counter intuitively, the size of the RRP does not predetermine the orientation of

48   presynaptic plasticity during high-frequency train since the calyx of Held with a very large

49   RRP (700 to 5000 SVs; Borst and Soria van Hoeve, 2012) immediately depress while

50   GC to Purkinje cell (PC) synapses facilitates during tens of APs (Kreitzer and Regehr,

51   2000; Valera et al., 2012; Schmidt et al., 2013), despite a RRP combining a small size

52   (4-8 SVs, Xu-Friedman et al., 2001) with a relatively high p_r (Schmidt et al., 2013; Sims

53   and Hartell, 2005; Valera et al., 2012 - but see Atluri and Regehr, 1996). Using computer

54   simulations associated with variance analysis of postsynaptic responses, we previously

55   showed that this striking facilitation is the consequence of an increase in *N* occurring in

56   milliseconds upon a Ca^{2+}-dependent process (Valera et al., 2012; Brachtendorf et al.,

57   2015). Here, we investigated the cellular mechanisms underlying presynaptic plasticity

58   at GC-PC synapses, not only during burst of activity but also upon fast changes in the

59   stimulation frequency. We did reveal the existence of two pools of mature SVs with

60   distinct releasable properties: the fully-releasable pool which can be released by a single

61   AP and the reluctant pool available for fusion in a millisecond time scale upon high-

62   frequency stimuli. Also, we showed that fully-releasable SVs can be specifically and

63   almost completely silenced by low-frequency stimulation. The ultrafast recruitment of

64   reluctant SVs underlies the large facilitation of glutamate release at high frequencies and

65   the rapid recovery of a full capacity of glutamate release following the almost complete

66   inactivation of fully-releasable SVs. We finally describe a model demonstrating how two

67   pools of SVs can account for the low-frequency depression and the ultrafast recovery of

68   glutamate release at high frequencies. These results support the idea that the

69   presynaptic machinery of GC boutons acts as a dynamic filter of GC activities, and

70   explain how a wide range of sensory inputs are computed within the cerebellar cortex.

71

MATERIALS AND METHODS

73   All experimental protocols are in accordance with European and French guidelines

74   for animal experimentation and have been approved by the Bas-Rhin veterinary office,

75   Strasbourg, France (authorization number A 67-311 to FD)

76   *Slice preparation.* Acute horizontal cerebellar slices were prepared from male

77   C57Bl/6 mice aged 18-25 days. Mice were anesthetized by isoflurane inhalation and

78 decapitated. The cerebellum was dissected out in ice-cold ACSF bubbled with carbogen

79 (95% O_2, 5% CO_2) and containing 120 mM NaCl, 3 mM KCl, 26 mM $NaHCO_3$, 1.25 mM

80 NaH_2PO_4, 2.5 mM $CaCl_2$, 2 mM $MgCl_2$, 10 mM glucose and 0.05 mM minocyclin. Slices

81 were then prepared (Microm HM650V) in a ice-cold solution containing 93 mM *N*-Methyl-

82 D-Glucamine, 2.5 mM KCl, 0.5 mM $CaCl_2$, 10 mM $MgSO_4$, 1.2 mM NaH_2PO_4, 30 mM

83 $NaHCO_3$, 20 mM HEPES, 3 mM Na-Pyruvate, 2mM Thiourea, 5 mM Na-ascorbate, 25

84 mM D-Glucose and 1 mM Kynurenic acid (Zhao et al., 2011). Slices 300 µm thick were

85 briefly soaked in a sucrose-based solution at 34°c bubbled with carbogen and containing

86 230 mM sucrose, 2.5 mM KCl, 26 mM $NaHCO_3$, 1.25 mM NaH_2PO_4, 25 mM glucose, 0.8

87 mM $CaCl_2$ and 8 mM $MgCl_2$ before being maintained in bubbled ASCF medium (see

88 above) at 34°C until their use for experiments.

89   *Electrophysiology.* After at least 1 h of recovery at 34°C, a slice was transferred to

90 a recording chamber. In order to block inhibitory transmission, postsynaptic plasticities,

91 $GABA_B$ and endocannabinoid signaling, slices were continuously perfused with bubbled

92 ACSF containing blockers of $GABA_A$, $GABA_B$, NMDA , CB1 and mGluR1 receptors. To

93 do so, the following antagonists were added: 100 µM picrotoxin, 10 µm CGP52432 (3-

94 [[(3,4-Dichlorophenyl)-methyl]amino]propyl(diethoxymethyl)phosphinic acid), 100 µM D-

95 AP5 (D-(-)-2-Amino-5-phosphonopentanoic acid) and 1 µM AM251 (1-(2,4-

96 Dichlorophenyl)-5-(4-iodophenyl)-4-methyl-N-(piperidin-1-yl)-1H-pyrazole-3-

97 carboxamide) and 2 µM JNJ16259685 ((3,4-Dihydro-2H-pyrano[2,3-b]quinolin-7-yl)-(cis-

98 4-methoxycyclohexyl)-methanone). Recordings were made at 34°C in PCs located in the

99 vermis. PCs were visualized using infrared contrast optics on an Olympus BX51WI

100 upright microscope. Whole-cell patch-clamp recordings were obtained using a

101 Multiclamp 700A amplifier (Molecular Devices). Pipette (2.5-3

102 MΩ resistance) capacitance was cancelled and series resistance (R_s) between 5 and 8

-4-

103   $m\Omega$ was compensated at 80%. R_s was monitored regularly during the experiment and

104   the recording was stopped when R_s changed significantly (> 20%). PCs were held at -60

105   mV. The intracellular solution for voltage-clamp recording contained 140 mM $CsCH_3SO_3$,

106   10 mM Phosphocreatine, 10 mM HEPES, 5 mM QX314-Cl, 10 mM BAPTA, 4 mM Na-

107   ATP and 0.3 mM Na-GTP. Parallel fibers were stimulated extracellularly using a

108   monopolar glass electrode filled with ACSF, positioned at least 100 μm away from the

109   PC to ensure a clear separation between the stimulus artifact and EPSCs. Pulse train

110   and low-frequency stimulation were generated using an Isostim A320 isolated constant

111   current stimulator (World Precision Instruments) controlled by WinWCP freeware (John

112   Dempster, Strathclyde Institute of Pharmacy and Biomedical Sciences, University of

113   Strathclyde, UK). The synaptic currents evoked in PCs were low-pass filtered at 2 KHz

114   and sampled at 100 KHz (National Instruments).

115   *Simulation of transmitter release and Ca^{2+} dynamics.* Models for Ca^{2+}-dependent

116   SVs fusion and replenishment (Millar et al., 2005; Wölfel et al., 2007; Sakaba, 2008)

117   were transformed into the corresponding ordinary differential equations and numerically

118   solved using Mathematica 10.0 (Wolfram Research).

119   Release rates were obtained by differentiation of the fused state. Paired-pulse

120   ratios were calculated from the ratios of release probabilities obtained by the integration

121   of release rates. Parameters for the release sensor part of the sequential two-pool

122   model (**Fig. 7A**, V, corresponding to the RRP) were similar to those used by Sakaba

123   (Sakaba, 2008) with forward rate k_{on} = $1*10^8$ $M^{-1}s^{-1}$, backward rate k_{off} = 3000 s^{-1},

124   cooperativity b = 0.25, and release rate γ = 5000 s^{-1}. Parameters for the replenishment

125   part of this model (R_0, R_1 representing the reluctant pool) were similar to those given by

126   Millar et al. (2005) for a phasic synapse and found by trial and error. The forward and

127   backward rate constants of Ca^{2+}-dependent priming and unpriming were $k_{prim} = 8*10^8$ M$^-$

128   ^{1}s^{-1} and $k_{unprim} = 120$ s^{-1}, respectively. Ca^{2+}-independent filling and unfilling rates were k_{fill}

129    $= 200$ s^{-1} and $k_{unfil} = 150$ s^{-1}, respectively. Ninety percent of released SVs were recycled

130   into the unprimed pool, supported by a slow Ca^{2+}-independent filling rate of $k_{basal} = 0.002$

131   s^{-1}, reflecting filling from a reserve pool. Recovery from Low-Frequency Depression

132   (LFD, see results section) was simulated by restarting the model at high frequency with

133   the size of the releasable pool set to the value at the end of the 2 Hz train, and the

134   unprimed pool (R_0) fully recovered. The one-pool model (**Fig. 7F**) and the parallel two-

135   pool model (**Fig. 7G**) and their parameters were taken from Wölfel et al. (2007).

136   Releases triggering Ca^{2+} signals were simulated as repeated Gaussian curves

137   spaced by the interstimulus intervals and adjusted to match the amplitude (22.5 μM) and

138   half-width (5 μs) of the estimated action potential-mediated Ca^{2+} signal at the release

139   sensor of PF synapses (Schmidt et al., 2013). In the sequential two-pool model (**Fig. 7A**)

140   SVs replenishment was driven by residual Ca^{2+} with an amplitude of 520 nM per pulse,

141   dropping exponentially with a time constant of 42 ms and summing linearly depending

142   on the length of the interstimulus interval (Brenowitz and Regehr, 2007). For the two

143   other models (**Fig. 7G,F**) SV replenishment occurred at a constant rate of 2 SV/ms

144   (Wölfel et al., 2007). Resting Ca^{2+} was assumed to be 50 nM.

145   *Data and statistical analysis.* Data were acquired using WinWCP 4.2.x freeware

146   (John Dempster, SIPBS, University of Strathclyde, UK). Analyses were performed using

147   PClamp9 (Molecular Devices), Igor (6.22A) graphing and analysis environment

148   (Wavemetrics, USA). Error bars in figures show SEMs. Student's *t* test or paired *t*-test

149   were performed when data were normally distributed; the Mann-Whitney Rank Sum Test

150   (MWRST) or the signed rank test were used in all other cases. Statistical tests were

151   performed using SigmaPlot 11 (Systat Software). The levels of significance are indicated

152   as *ns* (not significant) when p >0.05, * when $p \leq 0.05$, ** when $p \leq 0.01$ and *** when p

153   ≤ 0.001.

154

RESULTS

Low-Frequency depression at the granule cell-Purkinje cell synapse

In order to better understand the mechanisms underlying the large facilitation of glutamate release during repetitive activities at the GC-PC synapse, we first analyzed the behavior of synaptic transmission over a broad range of frequencies within transverse cerebellar slices prepared from young mice (P17 to P25). To focus our study on presynaptic mechanisms and rule out the possibility of postsynaptic contribution, we pharmacologically blocked the induction of postsynaptic long term plasticity (LTP and LTD), NMDA-dependent plasticity (Bidoret et al., 2009; Bouvier et al., 2016), and endocannabinoid signaling (Marcaggi and Attwell, 2005; Beierlein et al., 2007). We then stimulated parallel fibers (PF) with trains of stimuli (50 pulses) elicited at different frequencies (2, 50 and 100 Hz) and at near-physiological temperature (34°C) (**Fig. 1A**). As already reported in rodent cerebellar slices (Kreitzer and Regehr, 2000; Valera et al., 2012; Schmidt et al., 2013), a sustained facilitation of synaptic transmission was observed up to the 25th-30th stimulus at frequencies above 50 Hz, indicating that the number of SVs released increased with stimulation frequency. The paired-pulse facilitation (PPF) at the first interval increased with frequency (PPF $EPSC_2/EPSC_1$: 171.15% ± 10.03 at 50 Hz, n=9, 215.96% ± 6.90 at 100 Hz, n=27, **Fig. 1A**). After 30 to 40 stimuli, a depression ($EPSC_n/EPSC_1$ <1) was observed.

At many synapses, asynchronous release of quanta can be triggered by repeated activities (Rudolph et al., 2011; Kaeser and Regehr, 2013). Since asynchronous release can be detected by changes in the charge/amplitude ratio, we checked whether the charge and peak amplitude of EPSC evolved in similar ways during 50 Hz and 2 Hz stimulation. The perfect superimposition of normalized charges and amplitudes at any

179   stimulus number during 50 Hz and 2 Hz trains suggests that quanta released

180   asynchronously did not participate in a detectable way during theses protocols (**Fig. 1*A***).

181   This enables us to estimate the number of quanta released during these trains. Values

182   of quantal parameters found at unitary GC-PC synapses in mice (Schmidt et al., 2013)

183   were used to estimate the number of quanta released per varicosity at GC-PC synapse

184   during train a 2 Hz, 50 Hz and 100 Hz. The number of PFs stimulated in each

185   experiment was estimated by dividing the mean value of EPSC amplitude at 0.033 Hz by

186   the median EPSC amplitude obtained at unitary GC-PC synapse (5.3 pA, including

187   release failure, Schmidt et al., 2013). The number of quanta released during each

188   protocol was estimated by dividing the cumulative EPSC amplitude by the number of PF

189   stimulated and by the mean value of the quantal content obtained at unitary GC-PC

190   synapse (8 pA, Schmidt et al., 2013). Cumulative EPSC amplitude plots demonstrate

191   that the total number of quanta released is proportional to stimulation frequency.

192   However, although initial facilitation during the first two or three pulses is higher in 100

193   Hz train than in the 50 Hz train (Valera et al., 2012) no difference was observed in the

194   maximal recruitment of releasable SVs between 50 Hz and 100 Hz (number of quanta

195   released per bouton at 50 Hz = 39.47 ± 2.75, *n=9* compared to 40.14 ± 7.50 at 100 Hz,

196   *n=27*, *p*=0.82, *t*-test, **Fig. 1*B***).

197   At 2 Hz, the synaptic responses failed to facilitate (**Fig. 1*A, C***) and a sustained

198   stimulation of PF during hundreds of stimuli led to a near full blockage of synaptic

199   transmission (**Fig. *1D***). We named this rapid blockage of synaptic transmission "Low

200   Frequency Depression" (LFD). Strikingly, the time course of EPSC amplitude in all the

201   cells recorded (*n*=32) started to decrease mono-exponentially (**Fig. 1*E***, mean time

202   constant for depression at 2 Hz =15.9 s ± 1.2 s) after a median delay of 7 stimuli. It

203   should be noted that a lack of LFD was observed for less than 5% of PC recorded in the

204 vermis. These experiments were not taken in account for statistical analysis. Although it

205 has already been shown that action potential is faithfully initiated and transmitted along

206 parallel fibers at high frequencies and temperatures close to those in physiological

207 conditions (35°C), (Kreitzer and Regehr, 2000; Isope and Barbour, 2002; Baginskas et

208 al., 2009), repetitive extracellular stimulation of PF can induce decreases in fibers

209 excitability via strong accumulations of K+ in the extracellular space (Kocsis et al.,

210 1983). Hence, it could not be excluded that a decrease in the number of stimulated PF

211 underpinned part of the blockage observed during sustained 2 Hz stimulation. To

212 challenge this hypothesis, LFD was elicited by stimulating GC somata rather than PF

213 (**Fig. 1D**). The lack of any significant change in the onset and the kinetics of depression

214 after stimulating GC somata (**Fig. 1D-E**) suggested that change in PF excitability cannot

215 underlie LFD. This hypothesis also draws on several lines of evidences presented later

216 in figures 3, 4.

217 While the onset and the plateau of LFD were highly variable from one experiment

218 to another (**Fig. 1F**), these parameters stay stable for a given PC as long as the

219 recording of EPSCs could be maintained. In a series of 8 experiments, two LFD (LFD#1

220 and LFD#2) separated by a resting period of 5 to 10 minutes were successively elicited.

221 As shown in figure 1G, a full recovery of EPSC amplitude was achieved at the first

222 stimulus of LFD#2 elicited after the resting period (paired *t*-test performed on EPSC#1 of

223 LFD#1 and LFD#2, *p*=0.94, *n*=8). Strikingly, LFD#2 followed kinetics identical to LFD#1;

224 the similarity between LFD#1 and LFD#2 were confirmed by comparing the mean values

225 of EPSC amplitudes obtained at any stimulus number by a paired *t*-test. While LFD#1

226 and LFD#2 were statistically different when all stimuli were taken in account, we found

227 no statistical differences for the first 60 stimuli (*p*=0.081, *n*=8) corresponding to the main

228 time course of LFD (mean inhibition at stimulus #60: 66.8% ± 15.1%, *n*=8).

229   After pharmacologically blocking all known postsynaptic signaling events and

230   therefore excluding a main postsynaptic contribution in LFD, these findings reveal for the

231   first time that a sustained activity at low frequency can almost completely silences the

232   release apparatus at GC terminals.

233

234   **Immediate recovery from LFD by high-frequency trains**

235   Given the evidence that high-frequency trains of inputs can lead to the rapid

236   refilling of empty sites or even the recruitment of new active release sites (Saviane and

237   Silver, 2006; Hallermann et al., 2010; Valera et al., 2012; Chamberland et al., 2014), we

238   tested whether a full capacity of release could be recovered after LFD by an increase in

239   stimulation frequency. Alternatively, LFD may result from an activity-dependent blockage

240   of presynaptic voltage-dependent calcium channels (Xu and Wu, 2005). In the latter

241   case, accelerating the refilling of the RRP or increasing the number of release sites N

242   should not restore glutamate release after LFD. LFD was induced by 300 stimuli at 2 Hz,

243   and a train of 50 stimuli at 100 Hz was applied immediately after the last stimulus (**Fig.**

244   **2A**). After a full block of synaptic transmission, the recovery of glutamate release

245   capacity occurred within 10 ms (**Fig. 2B, C**) and was sustained throughout a train of 50

246   stimuli (mean recovery within 10 ms: 70.7% ± 7.6). Strikingly, EPSC amplitudes in this

247   100 Hz recovery train rapidly reached values observed at the same stimulus number in a

248   control train elicited before LFD induction (**Fig. 2C**), suggesting that the populations of

249   SVs recruited in these 2 conditions are the same or share the same release properties

250   (same size, same p_r). Mean amplitudes of EPSCs recorded during train at 50 Hz and

251   100 Hz applied in control condition and after LFD induction were compared (**Fig. 2D**).

252   Results showed that a full recovery from LFD was achieved within approximately 50 ms

253   or 5 stimuli at 50 Hz (normalized EPSC amplitude at the 5th stimulus: 203.67% ± 10.9 for

254 trains applied in control condition compared to 165.00% ± 21.29 for trains applied after

255 LFD, *p*=0.137, *t*-test, *n*=13) and 70 ms or 7 stimuli at 100 Hz (normalized EPSC

256 amplitude at the 7th stimulus: 207.24% ± 43.45 for trains applied in control condition

257 compared to 191.12% ± 49.72 for trains applied after LFD, *p*=0.181, MWRST, *n*=27).

258 We then studied how the frequency of stimulation in the train influenced the ability

259 of depressed synapses to recover a full capacity of release. Accordingly, 50 Hz and 20

260 Hz trains were applied after LFD and compared to 50 Hz and 20 Hz trains applied in

261 control conditions. Mean amplitudes of EPSCs recorded during train at 50 Hz applied in

262 control condition were not statistically different from those recorded after LFD induction

263 (**Fig. 2E**), but at 20 Hz the recovery was limited (**Fig. 2F**). Two hypotheses can explain

264 this ultrafast recovery of synaptic transmission following LFD: (1) a frequency-dependent

265 ultrafast replenishment of the RRP, or (2) the recruitment of a reluctant pool of SVs that

266 cannot be mobilized at low frequency as suggested in Valera et al. (2012).

267 **Recovery from LFD relies on the fast recruitment of reluctant SVs by a high-**

268 **frequency train**

269 In order to probe the existence of a reluctant pool supplying SVs to the fully-

270 releasable pool at high frequency, we checked whether the recovery from LFD by a 100

271 Hz train could be affected by a previous exhaustion of this reluctant pool. As our

272 previous results suggest that the reluctant pool can be recruited by short bursts at high

273 frequency (paired-pulse/triplet stimulation at 50 or 100 Hz, Valera et al., 2012), we

274 modified the paradigm of stimulation used to elicit LFD: LFD was induced by applying

275 100 triplets of stimulation instead of the 300 single pulses at 2 Hz (the total number of

276 stimuli is the same in both paradigms). The triplet frequency (from 10 to 200 Hz) was

277 changed during the experiment. This LFD was named LFD$_{triplet}$. Since LFD protocols can

278 be repeated several times after a recovery time (**Fig. 1F**), we systematically applied the

279   LFD and LFD$_{triplet}$ protocols to each PC recorded. Strikingly, although the number of

280   stimuli was the same in both type of protocols (LFD classic or LFD$_{triplet}$; **Fig. 3A, B**),

281   recovery from depression was highly influenced by triplet frequency: the higher the

282   frequency inside the triplets, the lower the level of recovery was seen to be (**Fig. 3B**).

283   For example, with triplets at 200 Hz during LFD$_{triplet}$, synaptic transmission hardly

284   recovers (maximal recovery 38.9 % ± 7.19 n=6, compared to 196.7 % ± 8.7, after LFD,

285   n=27, **Fig. 4C**), indicating that LFD$_{triplet}$ depleted or disabled the population of SVs that

286   support the recovery from LFD. If SVs 1) recruited only during LFD$_{triplet}$ (at the second

287   and third pulse of triplet stimulation) and 2) during recovery from LFD belong to the

288   same pool (reluctant pool), then the number of quanta released during LFD and LFD$_{triplet}$

289   should be the same. We performed a set of 18 experiments in which LFD and LFD$_{triplet}$

290   (triplets at 100 Hz) successively applied in the same cells were both followed by the

291   application of a 100 Hz recovery train (**Fig. 4A, B**). Cumulative EPSC amplitudes were

292   determined, and the approximate number of quanta released per bouton for the whole

293   protocol (LFD or LFD$_{triplet}$ + recovery train) was estimated (**Fig. 4C**). The normalized

294   cumulative EPSC amplitude was higher during LFD$_{triplet}$ than during LFD (6440.9% ±

295   945% for LFD compared to 9353.5% ± 1199.9% for LFD$_{triplet}$, p<0.001, paired t test,

296   n=18, **Fig. 4C, D**). However, when the cumulative EPSC amplitude during LFD or

297   LFD$_{triplet}$ was summed with the cumulative EPSC amplitude of the recovery train, no

298   further statistical differences were observed (11696.3% ± 1163.6 for LFD compared to

299   11379.0% ± 1349.6% for LFD$_{triplet}$, p=0.61, paired t test, n=18, **Fig. 4C, D**). The number

300   of quanta released during LFD was statistically lower than during LFD$_{triplet}$ (42.7 ± 6.2

301   quanta per varicosity for LFD compared to 60.8 ± 8.0 quanta per varicosity for LFD$_{triplet}$,

302   p<0.01, paired t-test, n=18, **Fig. 4E**). However, when the number of quanta released

303   during LFD or LFD$_{triplet}$ was summed with the number of quanta released during the

-13-

304 recovery train, no further statistical differences were observed (77.5 ± 7.7 quanta per

305 varicosity for LFD + recovery compared to 74.8 ± 8.9 quanta per varicosity for LFD$_{triplet}$ +

306 recovery, p=0.51, paired t-test, n=18, **Fig. 4E**). Moreover, the number of quanta

307 released during LFD and solely during recovery was statistically identical (42.7 ± 6.2

308 quanta per varicosity for LFD compared to 32.1 ± 2.3 quanta per varicosity for recovery,

309 p=0.1, paired t-test, n=18, **Fig. 4E**).These experiments indicate that the RRP in GC

310 boutons segregate in two distinct pools: the fully-releasable pool that can be released by

311 a single action potential and a reluctant pool that can only be recruited during bursts of

312 action potential reaching frequencies ≥ 50 Hz.

313 While it may seem improbable, it may be argued that LFD and recovery by 100

314 Hz train could result from fast changes in PF excitability (Kocsis et al., 1983). However,

315 the fact that 100 Hz trains are not able to reactivate synaptic transmission after LFD$_{triplet}$

316 is another argument as to why this hypothesis cannot be retained.

317 **A two-pool model accounts for basic experimental findings**

318 Our data suggest a segregation of SVs into different pools at GC terminals, which

319 is in line with several previous studies (Valera et al., 2012; Ishiyama et al., 2014;

320 Brachtendorf et al., 2015; Miki et al., 2016). They further suggest that SVs can be

321 recruited from a reluctant pool into an fully-releasable pool on a millisecond timescale.

322 Different previously published models could be suitable to account for these findings

323 (**Fig. 5**), including a sequential two-pool model with Ca^{2+}-dependent recruitment (Millar

324 et al., 2005; Sakaba, 2008), a single-pool model with Ca^{2+}-independent replenishment

325 and a parallel two-pool model with intrinsically different SVs in which both pools are

326 restored independently of Ca^{2+} (Wölfel et al., 2007; Schneggenburger et al., 2012). An

327 important demand on such model is that it needs to account for our experimental results

328 of high-frequency facilitation and LFD in a single model.

329   First, we analyzed a sequential two-pool model of release and Ca^{2+}-dependent

330   recruitment (Millar et al., 2005; Sakaba, 2008). In this model, release is triggered via a

331   Ca^{2+}-driven, five-site sensor from a fraction of releasable SVs (**Fig. 6A**, see Methods).

332   These SVs become replenished in two steps. The first step is a Ca^{2+}-dependent priming

333   step $(R_0 \rightarrow R_1)$, followed by a Ca^{2+}-independent filling step $(R_1 \rightarrow V)$, i.e. $R_0 + R_1$

334   corresponds to the reluctant pool and V to the fully-releasable pool in our experiments.

335   In the simulations, release was triggered by Gaussian shaped Ca^{2+} signals with

336   amplitudes of ~22 µM (Schmidt et al., 2013). Ca^{2+}-dependent recruitment was assumed

337   to be driven by residual Ca^{2+} (**Fig. 6B**) with an initial amplitude of 520 nM and a decay

338   constant of 42 ms (Brenowitz and Regehr, 2007). During high-frequency activation (100

339   Hz), this residual Ca^{2+} sums linearly (Brenowitz and Regehr, 2007), building up to a

340   steady state amplitude of ~2 µM across 50 stimuli. This high concentration of residual

341   Ca^{2+} drove rapid recruitment of SVs from the reluctant pool into the fully-releasable pool,

342   leading to a transient increase in the size of this pool (**Fig. 6C**; Valera et al., 2012).

343   Acting in concert with slow Ca^{2+} unbinding from the release sensor, which generates a

344   moderate facilitation on the ms timescale (Bornschein et al., 2013), SV recruitment

345   resulted in prolonged and facilitated release consistent with our experimental

346   observations (**Fig. 6D, E**, compared with **Fig. 1**). During low-frequency activation (2 Hz),

347   on the other hand, residual Ca^{2+} dropped back to its resting level between pulses and

348   recruited SVs returned to the unprimed pool prior to the next stimulus. This resulted in

349   the progressive depletion of fully-releasable SVs, leading to LFD. Renewed driving of

350   the depressed model at high frequency reproduced a rapid recovery from the

351   depression, and was followed by facilitation (**Fig. 6D** compared with **Fig. 2**), thus

352   illustrating the recruitment of the reluctant pool.

353   Next, we simulated release using a single pool model consisting of the "allosteric"

354   release sensor (Lou et al., 2005) supplemented with a replenishment step at a fixed,

355   Ca^{2+}-independent rate (one-pool model, Wölfel et al., 2007). Finally, we modeled release

356   using two parallel pools of releasable SVs differing in their intrinsic release rate

357   constants, thereby forming a pool of fast and a pool of slowly releasing vesicles (parallel

358   two-pool model, Wölfel et al., 2007). Both pools were replenished independent of Ca^{2+} at

359   a fixed rate as in the above single pool model. Notably, both the one-pool model and the

360   parallel two-pool model predict a depression of release during high-frequency activation

361   and a strong facilitation during sustained low-frequency stimulation (**Fig. 6*F,G***). This is in

362   stark contrast to our experimental results that showed the opposite behavior of GC

363   synapses. Thus, although the latter two models successfully described several aspects

364   of release at the depressing calyx of Held synapse that operates with a very large RRP

365   (Sätzler et al., 2002), it appears that the small cerebellar cortical GC synapse utilizes

366   different mechanisms to sustain release based on a small RRP and rapid, Ca^{2+} driven

367   recruitment.

368   Taken together, these findings show that several aspects of our experimental

369   findings, in particular high-frequency facilitation and LFD, can be reproduced by a simple

370   sequential two-pool model with Ca^{2+}-dependent recruitment but not, if recruitment is

371   assumed to be Ca^{2+}-independent. This does not exclude a contribution of more

372   sophisticated mechanisms like activity dependent a posteriori modifications (Wölfel et

373   al., 2007) or a separate facilitation sensor (Atluri and Regehr, 1996; Jackman et al.,

374   2016) but hints towards the minimal requirements for sustained release from a small

375   terminal operating with a small number of SVs in the RRP.

376   **Recovery from LFD depends on the size of both pools**

377   The sequential model predicts that the kinetics of refilling of the fully-releasable

378   pool after LFD depends on the size of in the reluctant pool. To test this hypothesis, we

379   determined the recovery kinetics of the fully-releasable pool after LFD (**Fig. 7A**, red

380   points) and LFD$_{triplet}$ (triplet at 200 Hz; **Fig. 7A**, blue points) by applying a single stimulus

381   at very low frequency (0.033 Hz) beginning 30 s after the end of the LFD protocol. As

382   shown in Figure 7A, full recovery after LFD is described by a single exponential function

383   (tau =153.8 s, R^2=0.93), indicating a single-step process. However, recovery following

384   LFD$_{triplet}$ was biphasic: during an initial phase, release remained almost fully blocked.

385   This initial phase was followed by a second phase that was again characterized by a

386   single exponential time course (tau = 212.8 s, **Fig. 7A**). Averaged time courses suggest

387   that the first phase could be considered as a delay, since a simple 90 s shift led to an

388   identical monoexponential recovery in both LFD (mean tau =156.3 s, R^2=0.98, *n*=8) and

389   LFD$_{triplet}$ (mean tau =149.3 s, R^2=0.96, *n*=6) (**Fig. 7B,C**). This set of experiments

390   suggests after depletion of both the reluctant and fully-releasable pools, the delay

391   preceding the exponential phase of recovery from depression (~90 s) might reflect the

392   time required to reconstitute the reluctant pool and then to refill the fully-releasable pool

393   from the reluctant pool.

394   To check this hypothesis, the following paradigm was designed: SVs from both

395   the reluctant and fully-releasable pools were released and inactivated by LFD$_{triplet}$

396   (triplets at 100 Hz), then a 100 Hz test train was applied after a variable resting period

397   (500 ms, 10 s or 1 min of rest after the end of LFD, **Fig. 7D**). The amplitudes of EPSCs

398   recorded in the test trains were compared to those obtained from the application of a

399   similar train in a control condition (before LFD). As shown in Figure 7D, the amplitude of

400   EPSCs during the test trains increased proportionally to the length of the resting period.

401   More interestingly, after 1 min of rest, the first responses in the test train were still fully

-17-

402   blocked (**Fig. 7E**) whereas the amplitudes of the late responses (after stimuli # 11-12 in

403   the test train) were similar to the corresponding responses in the control train (**Fig. 7F**).

404   This demonstrates that after 1 minute of rest, no SVs from the fully-releasable pool were

405   ready to be released, despite partial reconstitution of the reluctant pool and the

406   replenishment of the fully-releasable pool by the reluctant pool.

407

408   **Reluctant SVS can be recruited by increasing Ca^{2+} entry**

409   Finally, we investigated whether SVs in the reluctant pool are maintained in a low

410   probability state. If so, the reluctant pool could be affected by manipulations known to

411   affect p_r. We therefore studied the properties of LFD and of its recovery by 100 Hz train

412   after changes in p_r or by affecting the spaciotemporal profile of $[Ca^{2+}]$ through the use of

413   EGTA-AM (10 µM), a slow Ca^{2+} chelator that does not affect $[Ca^{2+}]$ in the nanodomain

414   during single AP but that may impair the building-up of $[Ca^{2+}]$ during high-frequency train

415   (Schmidt et al., 2013). Based on our work, increasing $[Ca^{2+}]_e$ from 2.5 mM (control

416   condition) to 4 mM leads p_r to increase from 0.25 to 0.67 for SVs in the fuly-releasable

417   pool (Valera et al., 2012). In the presence of 4 mM $[Ca^{2+}]_e$, LFD time course was barely

418   affected. Neither the delay (mean number of stimulus: 14.5 ± 2.8, n=30 at $[Ca^{2+}]_e$ = 2.5

419   mM compared to 17.6 ± 8.0, n=5, at $[Ca^{2+}]_e$, p=0.6, MWRST), nor the plateau of LFD

420   (mean percentage of initial responses: 14.2% ± 2.0%, n=30 at $[Ca^{2+}]_e$ = 2.5 mM

421   compared to 9.3% ± 1.4%, n=5, at $[Ca^{2+}]_e$=4 mM, p=0.69, MWRST) or the decay time

422   constant (tau: 14.3 s ± 1.3 s, n=30 at $[Ca^{2+}]_e$ = 2.5 mM compared to 18.9 s ± 6.8 s, n=5,

423   at $[Ca^{2+}]_e$=4 mM, p=0.87, MWRST) were statistically different in low and high Ca^{2+}

424   conditions   (**Fig. 8A, B**). At the opposite, recovery from LFD was strongly reduced

425   (maximal recovery 85.5 % ± 11.6 n=5, **Fig. 8B**) high Ca^{2+} condition. This indicates that

426   part of the reluctant pool was actually recruited during LFD upon increase in p_r. Finally,

427   we tested whether recruitment of the reluctant pool could be affected by impairing the

428   spaciotemporal profile of [Ca^{2+}]. Accordingly, LFD and the recovery form LFD by 100 Hz

429   train were probed before and after application of 10 µM EGTA-AM. As previously

430   showed, the application of 10 µM EGTA-AM did not affect the basal release of glutamate

431   (**Fig. 8C**). Also, while LFD time course was insensitive to EGTA-AM (p=0,61, paired t-

432   test performed on 3 successive EPSCs, n=9), the recovery from LFD was slightly slowed

433   down and reduced during the first responses of the 100 Hz train ; a statistical differences

434   could be detected only at stimulus #4 and #5 of the train (p=0.031 for both stimuli,

435   signed rank test, n=6) (**Fig. 8D**).

436   ## DISCUSSION

437   The present work demonstrates that the release of glutamate and presynaptic

438   plasticity at the GC-PC synapse are shaped by the existence of 2 pools of releasable

439   SVs, namely fully-releasable and reluctant SVs, bearing different properties for release.

440   Whether both pools belongs or not to the RRP is still a matter of debate (Pan and

441   Zucker, 2009; Neher, 2015) but if the RRP is restrained to SVs that can fuse with a

442   single AP, as proposed recently (Miki et al., 2016), then it would correspond only to fully-

443   primed SVs.

444   **Mechanism of recruitment of reluctant SVs**

445   Our results showed that reluctant SVs that cannot be recruited during single

446   stimuli at low-frequencies supports the release of glutamate during high-frequency train,

447   even after a full depletion of fully-releasable SVs (**Fig. 2-4**). At GC-PC synapses, the

448   localization of fusion events are restricted to distances that do not exceeds tens of

449   nanometers from presynaptic Ca^{2+} entry even during short burst at high frequencies

450   (Schmidt et al., 2013). The high speed of conversion (<10 ms) of reluctant SVs into fully

451 releasable SVs suggests that reluctant SVs are docked in the nanodomain as a physical

452 repositioning of reluctant SVs near the Ca^{2+}-channels (positional priming) is probably too

453 slow to occur with such fast kinetics.

454 The molecular mechanisms associated with the reluctant state and involved in the

455 fast recruitment of reluctant SVs at GC-PC synapses are unknown, and are beyond the

456 scope of this study. Our experiments suggest that fully-releasable SVs and reluctant

457 SVs differ by their Ca^{2+} sensitivity and that 2 Ca^{2+} sensors differentially shape glutamate

458 release during low- and fast-frequency stimulation (**Fig. 8**). In central synapses, the Ca^{2+}

459 sensors synaptotagmin 1, 2 and 9 are involved in fast synchronous release triggered by

460 a single AP (Xu et al., 2007) whereas synaptotagmin 7 which have slower kinetics for

461 binding Ca^{2+} is involved in delayed asynchronous release (Wen et al., 2010; Luo et al.,

462 2015). The recent finding that a lack of synaptotagmin 7 specifically impairs PPF without

463 affecting p_r (Jackman et al., 2016) makes this isoform as a good candidate for being

464 involved in reluctant mechanisms. In another hand, Munc13s, actin and myosin II

465 appears as good candidates for the fast recruitment of reluctant SVs. At the calyx of

466 Held, actin is involved in the recruitment of reluctant SVs after the depletion of the FRP

467 (Lee et al., 2012) and at GC-MLI synapses, actin and myosin II regulate the fast transfer

468 of SVs from a "transition pool" to a "docked pool" (Miki et al., 2016). In the same

469 synapses, the presence of Munc13s is required in a recently described "superpriming"

470 step that would correspond to the final maturation stage of fully-competent SVs (Lee et

471 al., 2013; Lipstein et al., 2013; Ishiyama et al., 2014). If we cannot exclude that identical

472 mechanisms underpin the transition between both pools at the GC-PC synapse, one

473 should keep in mind that this latter stands out by its large and sustained facilitation

474 during high-frequency trains while, at the opposite, depression dominate upon high

475 frequency stimulation at the calyx of Held and at some GC-MLI synapses

-20-

476   (Schneggenburger et al., 1999; Bao et al., 2010). This suggests that both organization of

477   SVs at the active zone and molecular mechanisms involved in the late stages of

478   exocytosis are different or optimized at GC-PC synapses.

479   Both experimental data (**Fig. 7**) and *in silico* simulation (**Fig. 6**) suggest that

480   reluctant SVs are recruited sequentially during high-frequency trains. Our model

481   proposes that SVs can reversibly shift from the fully-releasable status to the reluctant

482   one but do not explain why disequilibrium toward the reluctant state leading to LFD

483   occurs at 2 Hz and not at slower frequencies. Hence, while some experiments clearly

484   indicate that both pools are recruited sequentially (**Fig. 7**), one cannot exclude additional

485   "a posteriori" mechanisms impeding the functioning of active release sites in a range of

486   low frequencies (Wölfel et al., 2007; Schneggenburger et al., 2012). After SV fusion,

487   release sites have to be purged of SV membrane and the time course of this clearance

488   by endocytosis may act as a limiting factor for exocytosis during repetitive activities

489   (Hosoi et al., 2009; Hua et al., 2013). In another hand, as proposed in invertebrates

490   synapses (Silverman-Gavrila et al., 2005; Doussau et al., 2010), LFD may arise from an

491   imbalance in the activation of presynaptic kinases and phosphatases and as such the

492   kinase/phosphatase balance would act as a frequency sensor regulating the equilibrium

493   between the two pools.

494   Our estimation indicates that the number of SVs that can be released during high-

495   frequency trains after a full depletion of fully-releasable SVs corresponds to the size of

496   the reluctant pool (**Fig. 5**). Since the number of SVs released per bouton (30-40 SVs,

497   **Fig. 1,5**) during 50/100 Hz trains, LFD, LFD$_{triplet}$ or during recovery trains far exceeds the

498   number of docked SVs counted in one varicosity at GC-PC synapses (4-8 SVs, Xu-

499   Friedman et al., 2001), we postulate that the two releasable pools are refilled by other

500   pools (recycling pool, reserve pool) during LFD, LFD$_{triplet}$ and during the late phase of

-21-

501   high-frequency trains. Previous works performed in other cerebellar synapses suggest

502   that proteins of the cytomatrix (bassoon, actin, myosin II) (Hallermann et al., 2010;

503   Hallermann and Silver, 2013; Miki et al., 2016) in concert with a Ca^{2+}-driven

504   acceleration of replenishment kinetics trains (Saviane and Silver, 2006) participate to the

505   refilling of empty release sites during the last phase of high-frequency train.

506   **Segregation of releasable SVs in 2 pools shapes short-term plasticity**

507   Neuronal networks in the cerebellar cortex have to process sensory information

508   coded at ultra-high frequencies (up to 1 kilohertz, van Kan et al., 1993; Arenz et al.,

509   2008, 2009). Most of this information is conveyed to the granular layer, the input stage of

510   the cerebellar cortex, via the mossy fiber (MF) pathway. Strikingly, MF-GC synapses can

511   sustain high frequency trains of input by using a specific arrangement of the presynaptic

512   machinery to achieve ultra-fast reloading of SVs (Saviane and Silver, 2006; Rancz et al.,

513   2007; Hallermann et al., 2010; Ritzau-Jost et al., 2014). However, debate continues over

514   how these high frequencies inputs are integrated at the GC-PC synapses, the output

515   stage of the cerebellar cortex and the major site for information storage in the

516   cerebellum (Thach et al., 1992; Ito, 2006; D'Angelo and De Zeeuw, 2009). We already

517   showed that none of the classical mechanisms for facilitation (including the buffer

518   saturation model and residual Ca^{2+}, Pan and Zucker, 2009; Regehr, 2012) that predict a

519   pure increase in p_r during PPF can satisfactorily account for the high PPF at GC-PC

520   synapses and for its unusual ability to sustain glutamate release during tens of APs at

521   high-frequency trains. During a train of APs at high frequency, the local $[Ca^{2+}]$ at release

522   sites increases with AP number in the train (Schmidt et al., 2013; Miki et al., 2016)

523   leading to an immediate increase in N that underlies high values of PPF (Valera et al.,

524   2012; Brachtendorf et al., 2015). Here we showed that this increase in N arises from the

525   fast recruitment of reluctant SVs into the fully-releasable pool. A fast and sequential

526   recruitment of a "replacement pool" (analogous to the reluctant pool) in a docked pool

527   (analogous to the fully-releasable pool) accounting for PPF have been recently

528   described at GC-MLI synapses (Miki et al., 2016) but the GC-PC synapse is unique in so

529   far that the sequential recruitment of both pools is associated with the possibility to

530   specifically inactivate the fully-releasable pool by low-frequency stimulation. The

531   combination of both mechanisms gives the striking possibility to filter repetitive activities

532   around 2 Hz and to drastically invert the orientation of presynaptic plasticity (full

533   depression versus strong facilitation) in response to changes in the stimulation

534   frequency (**Fig. 2**). Finally, during high-frequency inputs, GC-PC synapses are able to

535   reset and standardized synaptic efficacy independently of the recent history of previous

536   events (**Fig. 2**).

537   **Physiological implications of the filtering of GC activity**

538   These results provide new hypotheses about information processing in the MF-

539   GC-PC pathway. *In vivo* experiments have shown that in lobules IV and V, GCs

540   responding to joint rotation receive spontaneous synaptic inputs from MF leading to

541   spontaneous firing at 2-10 Hz in GCs. Upon joint movement, GCs discharge shifts

542   instantaneously in burst mode with frequencies from ~50 Hz to 300 Hz (Jörntell and

543   Ekerot, 2006). Based on our work, we propose a model in which GC-PC synapses could

544   act as a filter of GC activity. In the absence of sensory input, GC inputs to PCs would be

545   filtered by an active silencing of presynaptic terminals. However, during joint movement,

546   the efficient transmission of high-frequency activity from MF to GC (Saviane and Silver,

547   2006; Rancz et al., 2007; Hallermann et al., 2010) and from GC to PC (Valera et al.,

548   2012), combined with the recruitment of the reluctant pool by high frequency trains at

549   GC-PC terminals, would allow a reliable transmission of sensory information to PC. In

550   such a model, the filtering of low-frequency activities originating from numerous GCs

551   would enhance the signal to noise ratio and help PC to recognize relevant inputs

552   generated by sensory inputs from spurious GC activities. Future studies could

553   investigate the response of inhibitory transmission, and more specifically feed-forward

554   inhibition, to the wide range of frequency observed in the GC firing pattern.

555

REFERENCES

Arenz A, Bracey EF, Margrie TW (2009) Sensory representations in cerebellar granule cells. Curr Opin Neurobiol 19:445–451 Available at: http://www.ncbi.nlm.nih.gov/pubmed/19651506 [Accessed November 26, 2013].

Arenz A, Silver RA, Schaefer AT, Margrie TW (2008) The contribution of single synapses to sensory representation in vivo. Science 321:977–980 Available at: http://www.pubmedcentral.nih.gov/articlerender.fcgi?artid=2771362&tool=pmcentrez&rendertype=abstract [Accessed November 21, 2013].

Atluri PP, Regehr WG (1996) Determinants of the time course of facilitation at the granule cell to Purkinje cell synapse. J Neurosci 16:5661–5671 Available at: http://www.ncbi.nlm.nih.gov/pubmed/8795622 [Accessed November 26, 2013].

Baginskas A, Palani D, Chiu K, Raastad M (2009) The H-current secures action potential transmission at high frequencies in rat cerebellar parallel fibers. Eur J Neurosci 29:87–96 Available at: http://www.ncbi.nlm.nih.gov/pubmed/19087162 [Accessed November 26, 2013].

Bao J, Reim K, Sakaba T (2010) Target-dependent feedforward inhibition mediated by short-term synaptic plasticity in the cerebellum. J Neurosci 30:8171–8179 Available at: http://www.ncbi.nlm.nih.gov/pubmed/20554867 [Accessed November 26, 2013].

Beierlein M, Fioravante D, Regehr WG (2007) Differential expression of posttetanic potentiation and retrograde signaling mediate target-dependent short-term synaptic plasticity. Neuron 54:949–959 Available at: http://www.pubmedcentral.nih.gov/articlerender.fcgi?artid=3251520&tool=pmcentrez&rendertype=abstract [Accessed November 25, 2013].

Bidoret C, Ayon A, Barbour B, Casado M (2009) Presynaptic NR2A-containing NMDA receptors implement a high-pass filter synaptic plasticity rule. Proc Natl Acad Sci U S A 106:14126–14131 Available at: http://www.pubmedcentral.nih.gov/articlerender.fcgi?artid=2729031&tool=pmcentrez&rendertype=abstract [Accessed February 26, 2015].

Bornschein G, Arendt O, Hallermann S, Brachtendorf S, Eilers J, Schmidt H (2013) Paired-pulse facilitation at recurrent Purkinje neuron synapses is independent of calbindin and parvalbumin during high-frequency activation. J Physiol 591:3355–3370 Available at: http://www.ncbi.nlm.nih.gov/pubmed/23671160 [Accessed November 15, 2013].

Borst JGG, Soria van Hoeve J (2012) The Calyx of Held Synapse: From Model Synapse to Auditory Relay. Annu Rev Physiol 74:199–224.

Bouvier G, Higgins D, Spolidoro M, Carrel D, Mathieu B, Léna C, Dieudonné S, Barbour B, Brunel N, Casado M (2016) Burst-Dependent Bidirectional Plasticity in the Cerebellum Is Driven by Presynaptic NMDA Receptors. Cell Rep:104–116 Available at: http://linkinghub.elsevier.com/retrieve/pii/S2211124716302285.
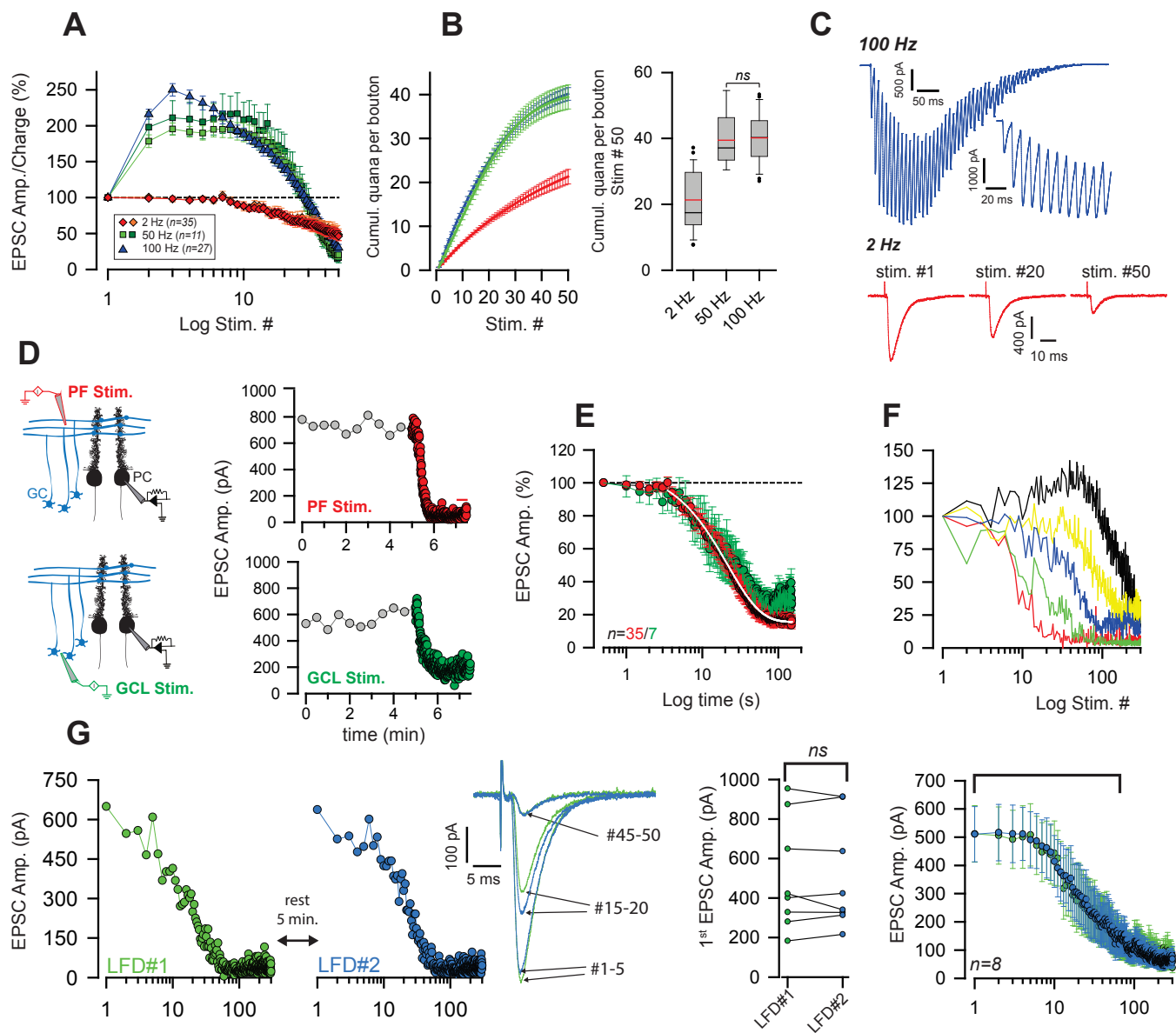
592 Brachtendorf S, Eilers J, Schmidt H (2015) A use-dependent increase in release sites drives facilitation at
593   calretinin-deficient cerebellar parallel-fiber synapses. Front Cell Neurosci 9:27 Available at:
594   http://www.pubmedcentral.nih.gov/articlerender.fcgi?artid=4315043&tool=pmcentrez&rendertyp
595   e=abstract [Accessed February 26, 2015].

596 Brenowitz SD, Regehr WG (2007) Reliability and heterogeneity of calcium signaling at single presynaptic
597   boutons of cerebellar granule cells. J Neurosci 27:7888–7898 Available at:
598   http://www.ncbi.nlm.nih.gov/pubmed/17652580 [Accessed November 26, 2013].

599 Chamberland S, Evstratova A, Tóth K (2014) Interplay between Synchronization of Multivesicular Release
600   and Recruitment of Additional Release Sites Support Short-Term Facilitation at Hippocampal Mossy
601   Fiber to CA3 Pyramidal Cells Synapses. J Neurosci 34:11032–11047 Available at:
602   http://www.ncbi.nlm.nih.gov/pubmed/25122902 [Accessed September 18, 2014].

603 D'Angelo E, De Zeeuw CI (2009) Timing and plasticity in the cerebellum: focus on the granular layer.
604   Trends Neurosci 32:30–40 Available at: http://www.ncbi.nlm.nih.gov/pubmed/18977038 [Accessed
605   September 19, 2014].

606 Doussau F, Humeau Y, Benfenati F, Poulain B (2010) A novel form of presynaptic plasticity based on the
607   fast reactivation of release sites switched off during low-frequency depression. J Neurosci
608   30:16679–16691 Available at: http://www.ncbi.nlm.nih.gov/pubmed/21148007 [Accessed
609   November 26, 2013].

610 Hallermann S, Fejtova A, Schmidt H, Weyhersmüller A, Silver RA, Gundelfinger ED, Eilers J (2010) Bassoon
611   speeds vesicle reloading at a central excitatory synapse. Neuron 68:710–723 Available at:
612   http://www.pubmedcentral.nih.gov/articlerender.fcgi?artid=3004039&tool=pmcentrez&rendertyp
613   e=abstract [Accessed November 10, 2013].

614 Hallermann S, Silver RA (2013) Sustaining rapid vesicular release at active zones: potential roles for
615   vesicle tethering. Trends Neurosci 36:185–194 Available at:
616   http://www.ncbi.nlm.nih.gov/pubmed/23164531 [Accessed November 15, 2013].

617 Hosoi N, Holt M, Sakaba T (2009) Calcium dependence of exo- and endocytotic coupling at a
618   glutamatergic synapse. Neuron 63:216–229 Available at:
619   http://www.ncbi.nlm.nih.gov/pubmed/19640480 [Accessed September 4, 2014].

620 Hua Y, Woehler A, Kahms M, Haucke V, Neher E, Klingauf J (2013) Blocking endocytosis enhances short-
621   term synaptic depression under conditions of normal availability of vesicles. Neuron 80:343–349
622   Available at: http://www.ncbi.nlm.nih.gov/pubmed/24139039 [Accessed January 29, 2014].

623 Ishiyama S, Schmidt H, Cooper BH, Brose N, Eilers J (2014) Munc13-3 Superprimes Synaptic Vesicles at
624   Granule Cell-to-Basket Cell Synapses in the Mouse Cerebellum. J Neurosci 34:14687–14696
625   Available at: http://www.jneurosci.org/cgi/doi/10.1523/JNEUROSCI.2060-14.2014 [Accessed
626   November 1, 2014].

627 Isope P, Barbour B (2002) Properties of unitary granule cell-->Purkinje cell synapses in adult rat cerebellar
628   slices. J Neurosci 22:9668–9678 Available at: http://www.ncbi.nlm.nih.gov/pubmed/12427822.

629 Ito M (2006) Cerebellar circuitry as a neuronal machine. Prog Neurobiol 78:272–303 Available at:
630   http://www.ncbi.nlm.nih.gov/pubmed/16759785 [Accessed November 13, 2013].

631 Jackman SL, Turecek J, Belinsky JE, Regehr WG (2016) The calcium sensor synaptotagmin 7 is required for
632   synaptic facilitation. Nature 529:88–91 Available at:
633   http://www.nature.com/doifinder/10.1038/nature16507\nhttp://www.ncbi.nlm.nih.gov/pubmed/
634   26738595.

635 Jörntell H, Ekerot C-F (2006) Properties of somatosensory synaptic integration in cerebellar granule cells
636   in vivo. J Neurosci 26:11786–11797 Available at: http://www.ncbi.nlm.nih.gov/pubmed/17093099
637   [Accessed November 23, 2013].

638 Kaeser PS, Regehr WG (2013) Molecular Mechanisms for Synchronous, Asynchronous, and Spontaneous
639   Neurotransmitter Release. Annu Rev Physiol 76:1–31 Available at:
640   http://www.pubmedcentral.nih.gov/articlerender.fcgi?artid=4503208&tool=pmcentrez&rendertyp
641   e=abstract [Accessed January 15, 2014].

642 Kocsis JD, Malenka RC, Waxman SG (1983) Effects of extracellular potassium concentration on the
643   excitability of the parallel fibres of the rat cerebellum. J Physiol 334:225–244 Available at:
644   http://doi.wiley.com/10.1113/jphysiol.1983.sp014491\nhttp://www.ncbi.nlm.nih.gov/pubmed/686
645   4558\nhttp://www.pubmedcentral.nih.gov/articlerender.fcgi?artid=PMC1197311.

646 Kreitzer a C, Regehr WG (2000) Modulation of transmission during trains at a cerebellar synapse. J
647   Neurosci 20:1348–1357 Available at: http://www.ncbi.nlm.nih.gov/pubmed/10662825.

648 Lee JS, Ho W-K, Lee S-H (2012) Actin-dependent rapid recruitment of reluctant synaptic vesicles into a
649   fast-releasing vesicle pool. Proc Natl Acad Sci U S A 109:E765–E774 Available at:
650   http://www.pubmedcentral.nih.gov/articlerender.fcgi?artid=3323990&tool=pmcentrez&rendertyp
651   e=abstract [Accessed July 20, 2014].

652 Lee JS, Ho W-K, Neher E, Lee S-H (2013) Superpriming of synaptic vesicles after their recruitment to the
653   readily releasable pool. Proc Natl Acad Sci U S A 110:15079–15084 Available at:
654   http://www.ncbi.nlm.nih.gov/pubmed/23980146 [Accessed December 3, 2013].

655 Lipstein N, Sakaba T, Cooper BH, Lin K-H, Strenzke N, Ashery U, Rhee J-S, Taschenberger H, Neher E,
656   Brose N (2013) Dynamic control of synaptic vesicle replenishment and short-term plasticity by
657   Ca(2+)-calmodulin-Munc13-1 signaling. Neuron 79:82–96 Available at:
658   http://www.ncbi.nlm.nih.gov/pubmed/23770256 [Accessed December 6, 2013].

659 Lou X, Scheuss V, Schneggenburger R (2005) Allosteric modulation of the presynaptic Ca2+ sensor for
660   vesicle fusion. Nature 435:497–501.

661 Luo F, Bacaj T, Südhof TC (2015) Synaptotagmin-7 Is Essential for Ca2+-Triggered Delayed Asynchronous
662   Release But Not for Ca2+-Dependent Vesicle Priming in Retinal Ribbon Synapses. J Neurosci
663   35:11024–11033 Available at: http://www.jneurosci.org/content/35/31/11024.abstract?etoc.

664 Marcaggi P, Attwell D (2005) Endocannabinoid signaling depends on the spatial pattern of synapse
665   activation. Nat Neurosci 8:776–781 Available at:
666   http://www.pubmedcentral.nih.gov/articlerender.fcgi?artid=2629534&tool=pmcentrez&rendertyp
667   e=abstract [Accessed November 22, 2013].

668 Miki T, Malagon G, Pulido C, Llano I, Neher E, Marty A (2016) Actin- and Myosin-Dependent Vesicle
669   Loading of Presynaptic Docking Sites Prior to Exocytosis. Neuron 91:808–823 Available at:
670   http://linkinghub.elsevier.com/retrieve/pii/S0896627316304184.

671 Millar AG, Zucker RS, Ellis-Davies GCR, Charlton MP, Atwood HL (2005) Calcium sensitivity of
672   neurotransmitter release differs at phasic and tonic synapses. J Neurosci 25:3113–3125 Available
673   at: http://www.ncbi.nlm.nih.gov/pubmed/15788768 [Accessed August 21, 2014].

674 Moulder KL, Mennerick S (2005) Reluctant vesicles contribute to the total readily releasable pool in
675   glutamatergic hippocampal neurons. J Neurosci 25:3842–3850 Available at:
676   http://www.ncbi.nlm.nih.gov/pubmed/15829636 [Accessed September 19, 2014].

677 Neher E (2015) Perspective Merits and Limitations of Vesicle Pool Models in View of Heterogeneous
678   Populations of Synaptic Vesicles. Neuron 87:1131–1142 Available at:
679   http://dx.doi.org/10.1016/j.neuron.2015.08.038.

680 Pan B, Zucker RS (2009) A General Model of Synaptic Transmission and Short-Term Plasticity. Neuron
681   62:539–554 Available at: http://dx.doi.org/10.1016/j.neuron.2009.03.025.

682 Rancz E a, Ishikawa T, Duguid I, Chadderton P, Mahon S, Häusser M (2007) High-fidelity transmission of
683   sensory information by single cerebellar mossy fibre boutons. Nature 450:1245–1248 Available at:
684   http://www.ncbi.nlm.nih.gov/pubmed/18097412 [Accessed November 26, 2013].

685 Regehr WG (2012) Short-term presynaptic plasticity. Cold Spring Harb Perspect Biol 4:a005702 Available
686   at: http://www.ncbi.nlm.nih.gov/pubmed/22751149 [Accessed December 3, 2013].

687 Ritzau-Jost A, Delvendahl I, Rings A, Byczkowicz N, Harada H, Shigemoto R, Hirrlinger J, Eilers J,
688   Hallermann S (2014) Ultrafast action potentials mediate kilohertz signaling at a central synapse.
689   Neuron 84:152–163 Available at:
690   http://www.sciencedirect.com/science/article/pii/S0896627314007375 [Accessed October 13,
691   2014].

692 Rudolph S, Overstreet-Wadiche L, Wadiche JI (2011) Desynchronization of multivesicular release
693   enhances Purkinje cell output. Neuron 70:991–1004 Available at:
694   http://www.pubmedcentral.nih.gov/articlerender.fcgi?artid=3148031&tool=pmcentrez&rendertyp
695   e=abstract [Accessed June 26, 2014].

696 Sakaba T (2006) Roles of the fast-releasing and the slowly releasing vesicles in synaptic transmission at
697   the calyx of held. J Neurosci 26:5863–5871 Available at:
698   http://www.ncbi.nlm.nih.gov/pubmed/16738227 [Accessed November 23, 2013].

699 Sakaba T (2008) Two Ca(2+)-dependent steps controlling synaptic vesicle fusion and replenishment at the
700   cerebellar basket cell terminal. Neuron 57:406–419 Available at:
701   http://www.ncbi.nlm.nih.gov/pubmed/18255033 [Accessed November 26, 2013].

702 Sakaba T, Neher E (2001) Preferential potentiation of fast-releasing synaptic vesicles by cAMP at the
703   calyx of Held. Proc Natl Acad Sci U S A 98:331–336 Available at:
704   http://www.pubmedcentral.nih.gov/articlerender.fcgi?artid=14590&tool=pmcentrez&rendertype=
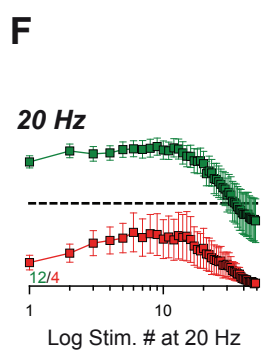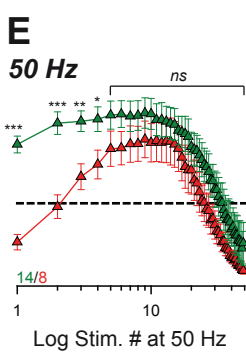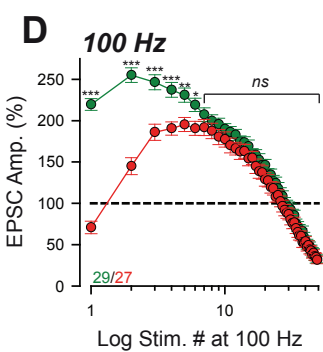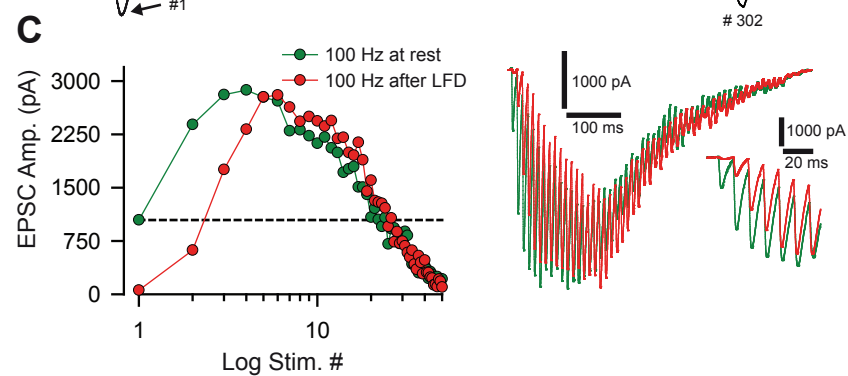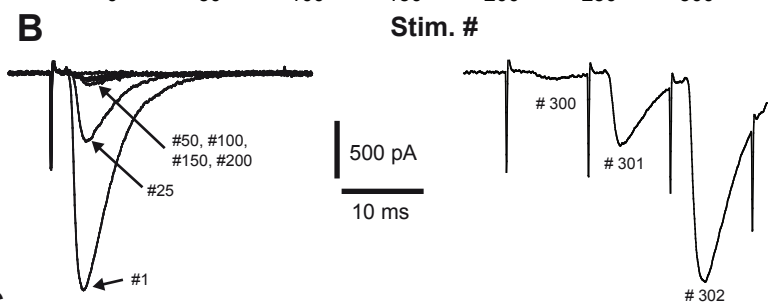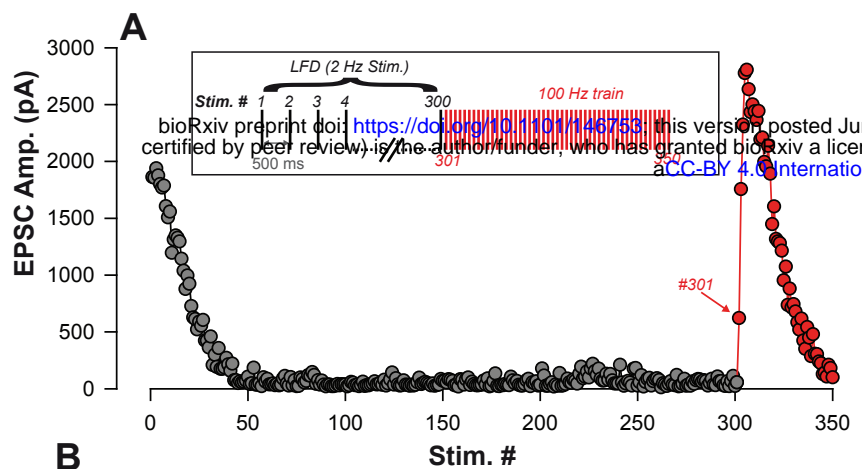705   abstract.

706   Sätzler K, Söhl LF, Bollmann JH, Borst JGG, Frotscher M, Sakmann B, Lübke JHR (2002) Three-dimensional
707   reconstruction of a calyx of Held and its postsynaptic principal neuron in the medial nucleus of the
708   trapezoid body. J Neurosci 22:10567–10579 Available at:
709   http://www.ncbi.nlm.nih.gov/pubmed/12486149 [Accessed December 4, 2013].

710   Saviane C, Silver RA (2006) Fast vesicle reloading and a large pool sustain high bandwidth transmission at
711   a central synapse. Nature 439:983–987 Available at:
712   http://www.ncbi.nlm.nih.gov/pubmed/16496000 [Accessed November 26, 2013].

713   Schmidt H, Brachtendorf S, Arendt O, Hallermann S, Ishiyama S, Bornschein G, Gall D, Schiffmann SN,
714   Heckmann M, Eilers J (2013) Nanodomain coupling at an excitatory cortical synapse. Curr Biol
715   23:244–249 Available at: http://www.ncbi.nlm.nih.gov/pubmed/23273895 [Accessed August 28,
716   2015].

717   Schneggenburger R, Han Y, Kochubey O (2012) Ca2+ channels and transmitter release at the active zone.
718   Cell Calcium 52:199–207 Available at: http://dx.doi.org/10.1016/j.ceca.2012.04.011.

719   Schneggenburger R, Meyer AC, Neher E (1999) Released fraction and total size of a pool of immediately
720   available transmitter quanta at a calyx synapse. Neuron 23:399–409 Available at:
721   http://linkinghub.elsevier.com/retrieve/pii/S0896627300807898 [Accessed May 26, 2015].

722   Silverman-Gavrila LB, Orth PMR, Charlton MP (2005) Phosphorylation-dependent low-frequency
723   depression at phasic synapses of a crayfish motoneuron. J Neurosci 25:3168–3180 Available at:
724   http://www.ncbi.nlm.nih.gov/pubmed/15788774 [Accessed December 6, 2013].

725   Sims RE, Hartell N a (2005) Differences in transmission properties and susceptibility to long-term
726   depression reveal functional specialization of ascending axon and parallel fiber synapses to Purkinje
727   cells. J Neurosci 25:3246–3257 Available at: http://www.ncbi.nlm.nih.gov/pubmed/15788782
728   [Accessed March 27, 2014].

729   Thach WT, Goodkin HP, Keating JG (1992) The cerebellum and the adaptive coordination of movement.
730   Annu Rev Neurosci 15:403–442 Available at: http://www.ncbi.nlm.nih.gov/pubmed/1575449
731   [Accessed August 19, 2014].

732   Valera AM, Doussau F, Poulain B, Barbour B, Isope P (2012) Adaptation of granule cell to Purkinje cell
733   synapses to high-frequency transmission. J Neurosci 32:3267–3280 Available at:
734   http://www.ncbi.nlm.nih.gov/pubmed/22378898 [Accessed April 23, 2015].

735   Van Kan PL, Gibson a R, Houk JC (1993) Movement-related inputs to intermediate cerebellum of the
736   monkey. J Neurophysiol 69:74–94 Available at: http://www.ncbi.nlm.nih.gov/pubmed/8433135.

737   Wen H, Linhoff MW, McGinley MJ, Li G, Corson GM, Mandel G, Brehm P (2010) Distinct roles for two
738   synaptotagmin isoforms in synchronous and asynchronous transmitter release at zebrafish
739   neuromuscular junction. Proc Natl Acad Sci U S A 107:13906–13911 Available at:
740   http://eutils.ncbi.nlm.nih.gov/entrez/eutils/elink.fcgi?dbfrom=pubmed&id=20643933&retmode=re
741   f&cmd=prlinks\npapers3://publication/doi/10.1073/pnas.1008598107.

742   Wölfel M, Lou X, Schneggenburger R (2007) A mechanism intrinsic to the vesicle fusion machinery
743   determines fast and slow transmitter release at a large CNS synapse. J Neurosci 27:3198–3210
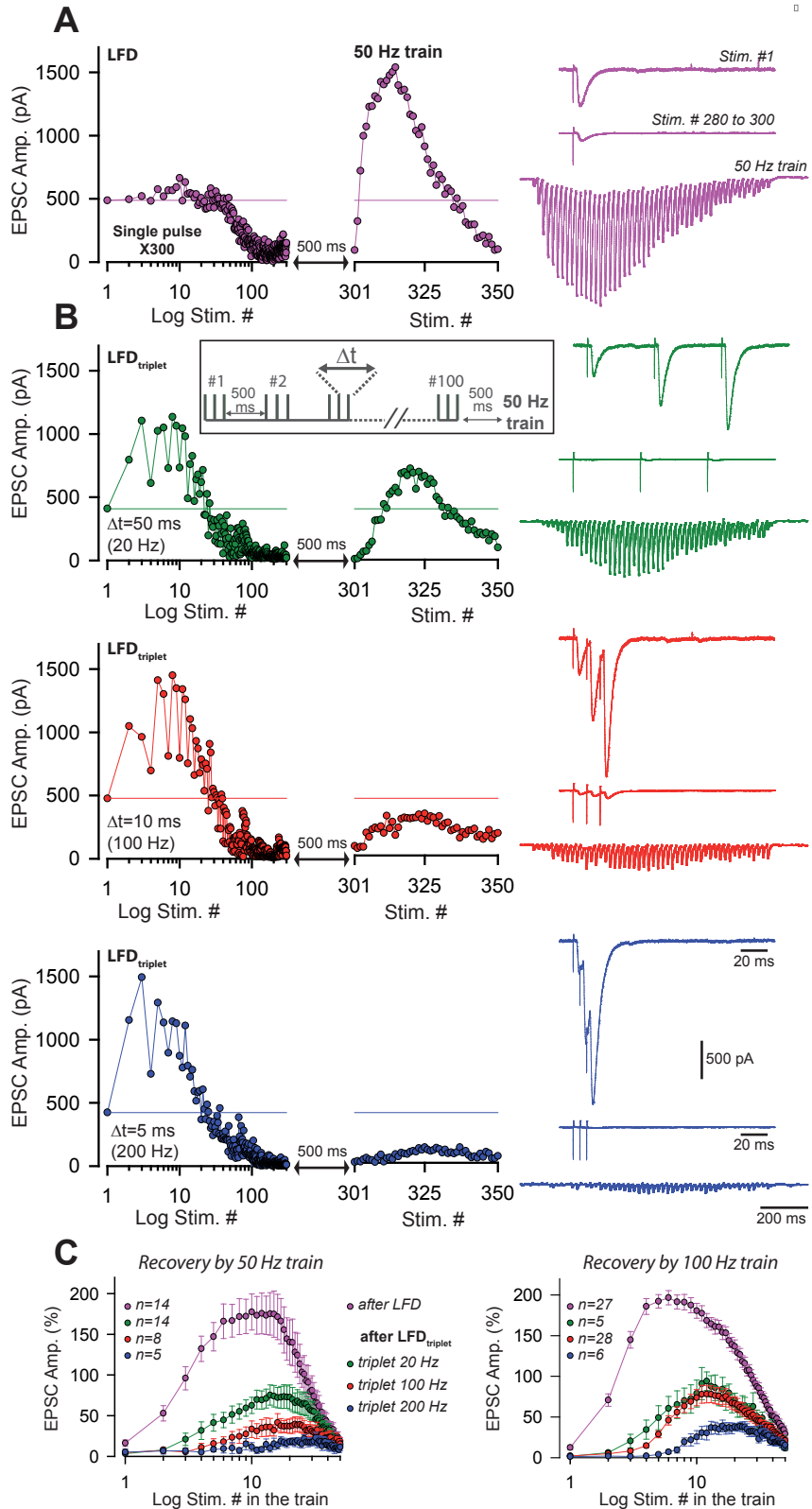744   Available at: http://www.ncbi.nlm.nih.gov/pubmed/17376981 [Accessed November 15, 2013].

745 Xu J, Mashimo T, S??dhof TC (2007) Synaptotagmin-1, -2, and -9: Ca2+ Sensors for Fast Release that
746   Specify Distinct Presynaptic Properties in Subsets of Neurons. Neuron 54:567–581.

747 Xu J, Wu L-G (2005) The decrease in the presynaptic calcium current is a major cause of short-term
748   depression at a calyx-type synapse. Neuron 46:633–645 Available at:
749   http://www.ncbi.nlm.nih.gov/pubmed/15944131 [Accessed December 3, 2013].

750 Xu-Friedman M a, Harris KM, Regehr WG (2001) Three-dimensional comparison of ultrastructural
751   characteristics at depressing and facilitating synapses onto cerebellar Purkinje cells. J Neurosci
752   21:6666–6672 Available at: http://www.ncbi.nlm.nih.gov/pubmed/11517256.

753 Zhao S, Ting JT, Atallah HE, Qiu L, Tan J, Gloss B, Augustine GJ, Deisseroth K, Luo M, Graybiel AM, Feng G
754   (2011) Cell type–specific channelrhodopsin-2 transgenic mice for optogenetic dissection of neural
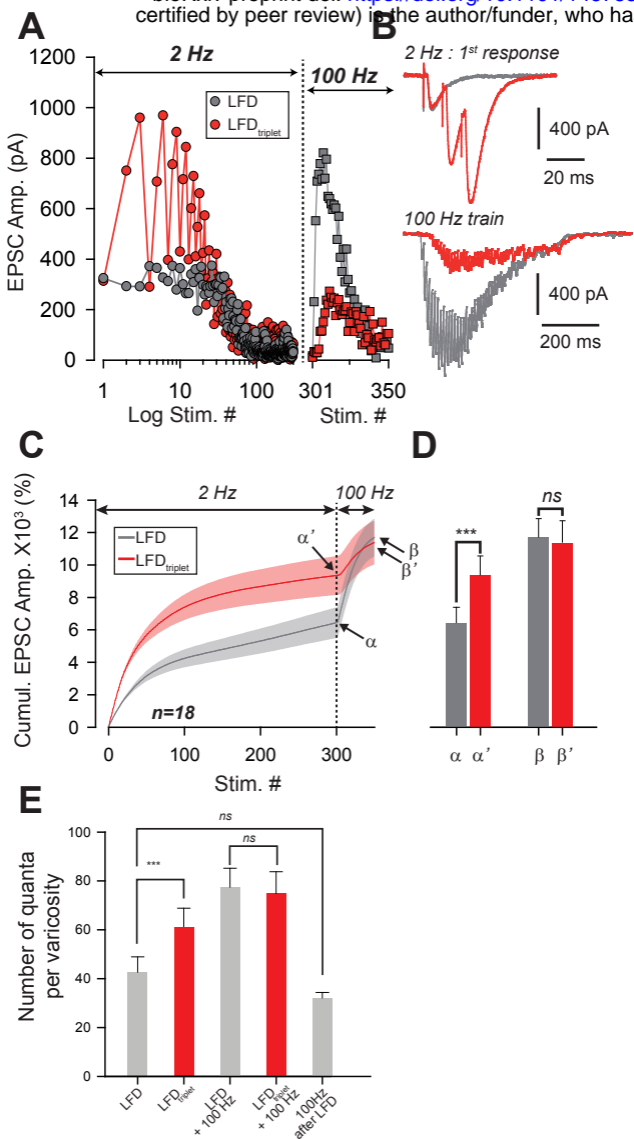755   circuitry function. Nat Methods 8:745–752 Available at:
756   http://www.nature.com/doifinder/10.1038/nmeth.1668 [Accessed November 7, 2013].

757

A

EPSC Amp./Charge (%)

- 2 Hz (*n=35*)
- 50 Hz (*n=11*)
- 100 Hz (*n=27*)

Log Stim. #

B

Cumul. quana per bouton

Stim. #

Cumul. quana per bouton Stim # 50

ns

2 Hz   50 Hz   100 Hz

C

100 Hz

500 pA
50 ms

1000 pA
20 ms

2 Hz

stim. #1   stim. #20   stim. #50

400 pA
10 ms

D

PF Stim.

GC   PC

GCL Stim.

PF Stim.

GCL Stim.

EPSC Amp. (pA)

time (min)

E

EPSC Amp. (%)

n=35/7

Log time (s)

F

Log Stim. #

G

EPSC Amp. (pA)

LFD#1

rest
5 min.

LFD#2

100 pA
5 ms

#45-50

#15-20

#1-5

1st EPSC Amp. (pA)

ns

LFD#1   LFD#2

EPSC Amp. (pA)

n=8

Doussau *et al*, Fig. 1

Doussau *et al*, Fig. 2

Doussau *et al*, Figure 3

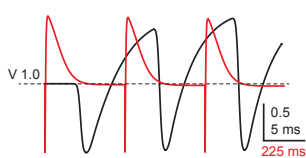**Doussau *et al*, Fig. 4**
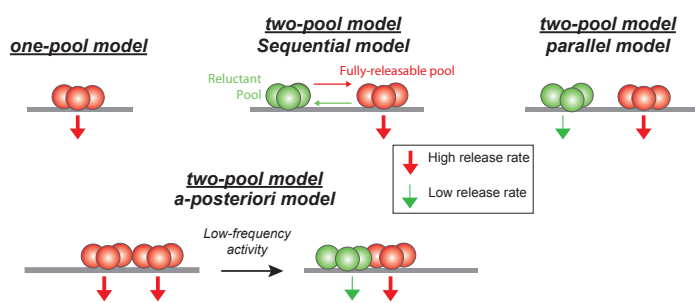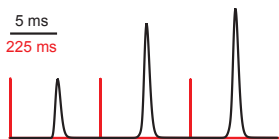
Doussau *et al*, Fig. 5

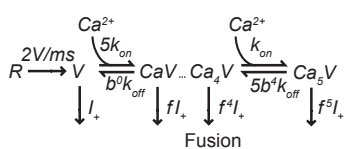## A Sequential mode (two-pool model)
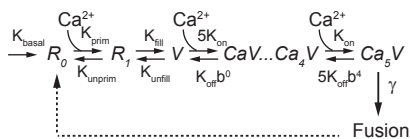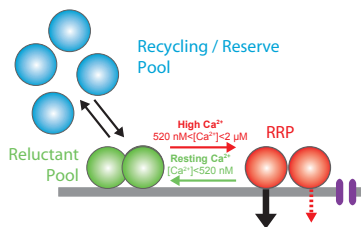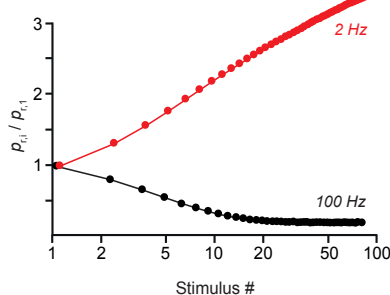

B

Local Ca²⁺ at release sensor
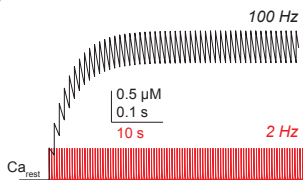
C

D

E
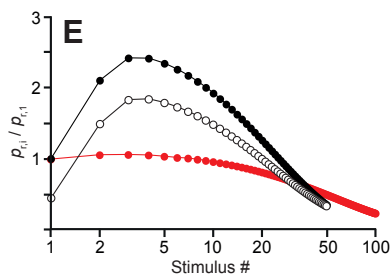
F One-pool model
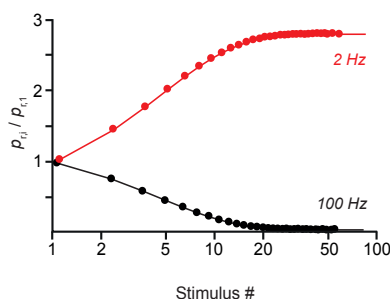
G Parallel mode (two-pool model)
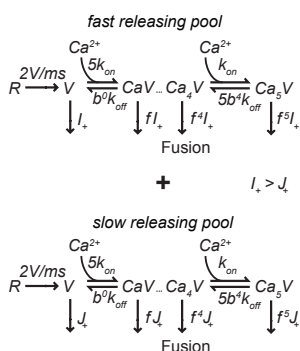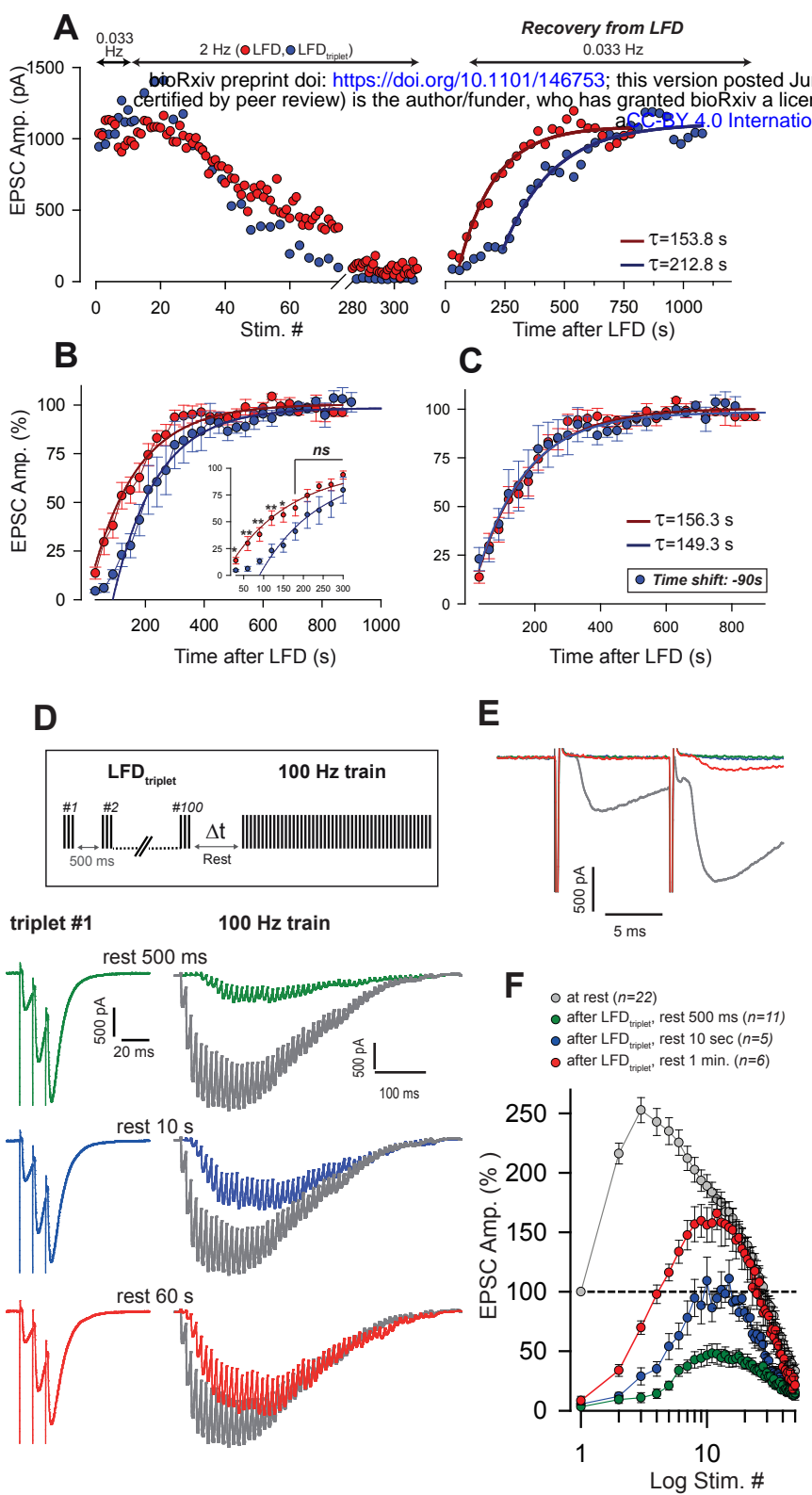
Doussau *et al*, Fig. 6
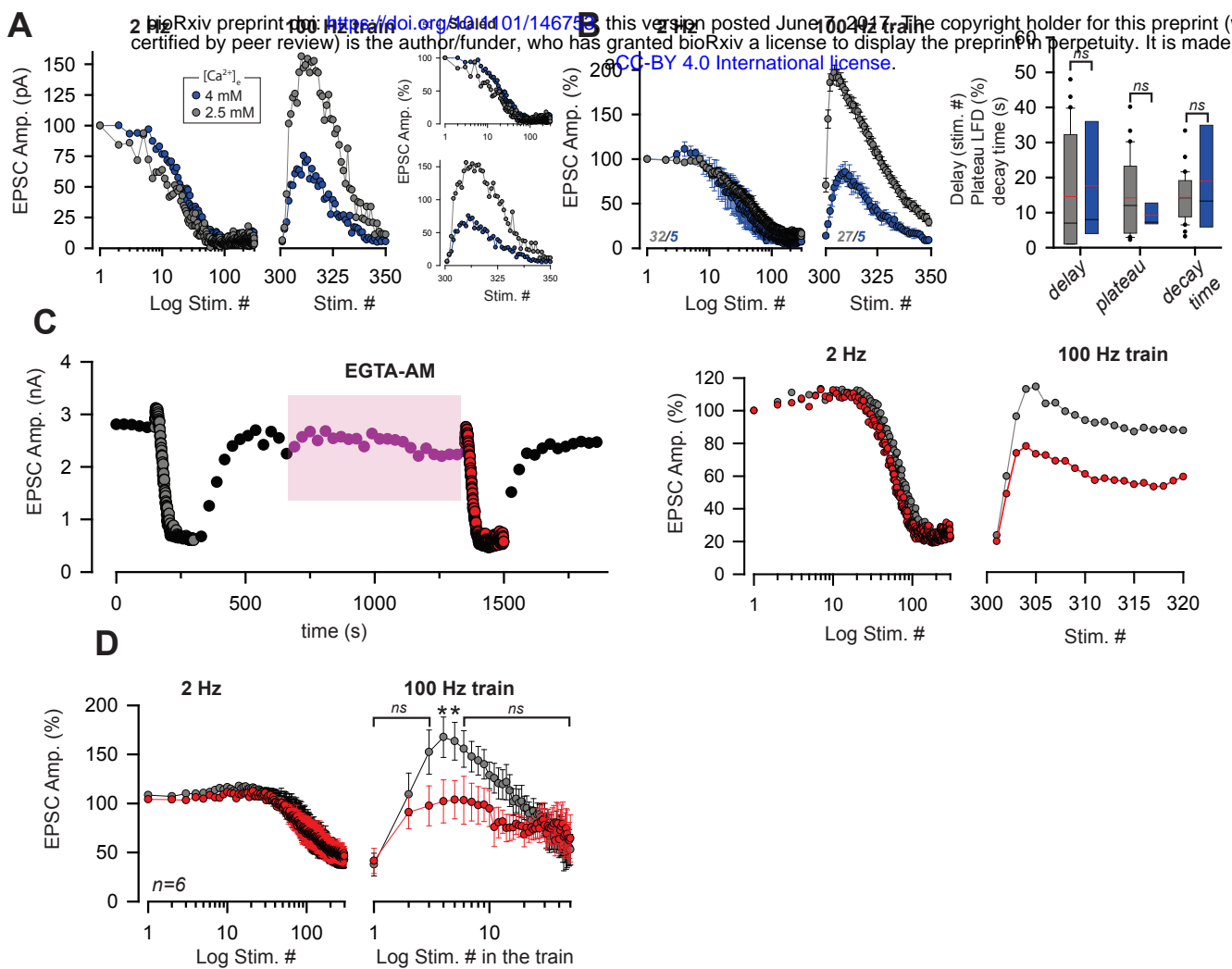
Doussau *et al*, Fig. 7

Doussau *et al*, Fig. 8

LEGENDS

Figure 1. Low-frequency depression at GC-PC synapses. **A,** Averaged EPSC amplitude and charge versus stimulus number during train of stimuli at 2, 50 and 100 Hz. At 50 Hz EPSC amplitude and EPSC charge are represented with light green squares and dark green squares respectively. At 2 Hz, EPSC amplitudes and EPSC charge are represented with red diamonds and orange diamonds respectively. Due to the overlapping of EPSC, charge values were not measured at 100 Hz. Note the absence of facilitation at 2 Hz. **B,** Corresponding cumulative plots of the number of quanta release per bouton (left). The cumulative number of quanta released at 50 Hz and 100 Hz at the 50th stimulus were statistically identical (t-test, p=0.82). Mean and median lanes are respectively represented in red and black (right) **C,** Examples of EPSCs during train at 100 Hz and 2 Hz. *Inset*: The first EPSCs observed during 100 Hz train application. The stimulus artifacts have been subtracted for the 100 Hz train. **D,** Time course of EPSC amplitude following stimulation of PF (upper panels) or GC somata (lower panels) at 0.033 Hz (gray points) and 2Hz (red or green points) **E,** Mean normalized EPSC amplitude during sustained 2 Hz stimulation of PF (red points) or GC somata (green points). Note the delay before the actual induction of depression. The depression was fitted by a monoexponential function (tau = 21.7 s, white lane). **F,** Selected time course of LFD recorded in 5 PCs showing differences in the onset and the plateau of depression **G,** Left graph: Time courses of two successive LFDs elicited in the same cell. The second LFD (LFD#2, blue points) was elicited after a resting period of 5 minutes after the first had ended (LFD#1, green points). Traces correspond to averaged EPSCs recorded during LFD#1 and LFD#2 (green and blue traces, respectively) at the indicated stimulus numbers. Middle graph: Values of EPSC amplitude recorded at the 1st stimuli of LFD#1 (green points) and LFD#2 (blue points).The lack of statistical difference

(*p*=0.94, paired *t*-test, *n*=8) in EPSC amplitudes between LFD#1 and LFD#2 reflects a full recovery from depression after the resting period that followed LFD#1. Right graph: Superimposition of mean EPSC amplitudes recorded during LFD#1 (green points) and LFD#2 (blue points). The similarity between LFD#1 and LFD#2 was tested using a paired *t*-test. The values were statistically different for the entire experiment (p<0.001, *n*=8) but the 60 firsts response were statistically identical (paired *t*-test, *p*=0.08, *n*=8).

Figure 2. Ultrafast recovery from LFD by high-frequency trains. **A,** Typical experiment illustrating EPSC amplitude during LFD (gray points, stimulation at 2 Hz) and the fast recovery from LFD via high-frequency trains (red points, stimulation 100 Hz). *Inset*: protocol of stimulation. Stimulus #1 denotes the beginning of 2 Hz stimulation. **B,** Superimposed EPSC recorded during 2 Hz stimulation (left) and during the following 100 Hz train (right) at the indicated stimulus number. Note the ultrafast recovery from depression at 100 Hz (stimulus # 301). **C,** Left, Example of time course of EPSC amplitudes plotted against stimulus number during 100 Hz train applied in the control condition (green), or starting 10 ms after 300 stimuli at 2 Hz. EPSCs were recorded in the same PC. The dashed line corresponds to the baseline amplitude (mean value of EPSC at 0.033 Hz). Note the superposition of EPSC amplitudes after the 4th stimuli at 100 Hz. Right, Corresponding traces recorded during these 100 Hz trains. *Inset*: The first EPSCs observed during train application. **D,** Mean values of normalized EPSC amplitude elicited by trains of stimulation at 100 Hz, 50 Hz and 20 Hz at baseline (0.033 Hz, green) or after LFD induction (2 Hz, red). EPSC amplitudes were not significantly different after the 7th stimuli for 100 Hz trains (MWRST, *p*=0.181, *n*=27) and after the 5th stimuli for 50 Hz trains (*t*-test, *p*=0.137, *n*=13). Numbers at the bottom of the graphs indicate the number of cells for each condition.

Figure 3. Short-term facilitation during triple-pulse stimulation at high frequency impedes recovery from LFD via high-frequency trains. *A,* LFD induced by a single pulse followed by a 50 Hz train *B,* LFDs induced by a triple pulse at different frequencies (LFD$_{triplet}$, see inset for protocol), namely 20 Hz (green), 100 Hz (red) and 200 Hz (blue) followed by a 50 Hz train. For each condition, the upper traces correspond to EPSCs recorded at stimulus #1 (purple trace) or at triple pulse #1 (other traces) of the 2 Hz stimulation. The middle traces correspond to averaged EPSCs recorded during the LFD plateau (stimuli #280 to #300 for the purple trace and triple-pulses #80 to #100 for other traces). The bottom traces from which stimulus artifacts were subtracted correspond to EPSCs recorded during the 50 Hz train applied 500 ms after the 2 Hz stimulation ended. All data and traces were obtained in the same PC, and LFDs were elicited after a resting period of 5 minutes after the end of each protocol. *C,* Mean values of normalized EPSC amplitude plotted against stimulus number and recorded during 50 Hz train (left) and 100 Hz train applied 500 ms after LFD induction (300 single stimuli at 2 Hz or 100 triple pulses at 2 Hz). Color code is identical to that used in *A, B.*

Figure 4. Recruitment of reluctant vesicles by high-frequency trains underpins recovery from LFD. *A,* Superimposition of the ESPC amplitude time courses elicited during LFD induction (gray circles) or LFD$_{triplet}$ (triplet stimulation at 100 Hz, red circles) in the same PC, and during the recovery from LFD via application of a 100 Hz train (gray squares for a 100 Hz train applied 500 ms after LFD, and red squares for a 100 Hz train applied 500 ms after LFD$_{triplet}$). *B,* The upper traces correspond to the superimposition of the first EPSCs recorded at stimulus #1 for LFD (gray trace) and LFD$_{triplet}$ (red trace). The lower traces correspond to EPSCs recorded during the 100 Hz trains applied 500 ms after LFD (gray trace) or 500 ms after LFD$_{triplet}$. *C,* Mean values of the cumulative EPSC amplitudes during LFD and LFD$_{triplet}$ induction protocol followed by a recovery

train at 100 Hz (n=18 cells). LFD and LFD$_{triplet}$ were elicited successively in the same PCs. The dashed line indicates the beginning of the 100 Hz trains. α and α' correspond to the cumulative value at the end of LFD protocols, β and β' are values obtained following the recovery trains. **D,** Mean values of α, α', β and β' (same y axis as in *C*). **E,** Estimation of the number of quanta released per varicosity at GC-PC synapse during LFD, LFD$_{triplet}$ and during the recovery via 100 Hz train (same set of experiments than in *D*). For the panels *D* and *E*, data were compared by using paired *t*-test.

Figure 5. Schematics of the various models accounting for exocytosis at GC-PC synapses. Based on hypothesis proposed in other synapses, exocytosis could be achieved through an intrinsically homogeneous pool of release-ready SVs (one-pool model) or through a two-pool model with alternative stages of transition between the two pools. For the two-pool model, releasable SVs are separated in a fully-releasable pool (red SVs) or a reluctant one (green SVs).

Figure 6. Models of facilitation and LFD. **A,** Scheme illustrating the sequential model of Ca^{2+} binding and release at the PF-PC synapse (left). Voltage-dependent calcium channels are represented in purple. In the corresponding mathematical model (right) the recycling / reserve pool is contained only implicitly by restoration of the reluctant pool (R$_0$+R$_1$) from fused SVs (dashed arrow) and via a basal refilling rate (k_{basal}). Therefore, this model is referred to as sequential "two-pool" model. During high-frequency activation the residual Ca^{2+} increases, resulting in recruitment of SVs from the reluctant pool into the RRP, i.e. a temporal increase in the RRP that causes substantial facilitation (red arrow). The residual Ca^{2+} generates an additional moderate, short-lasting facilitation due to slow unbinding from the release sensor (dashed red arrow). During low frequency activation at 2 Hz, the residual Ca^{2+} fully drops back to resting level between stimuli and SVs recruited to the RRP return to the reluctant pool

(green arrow). ***B,*** Simulated time courses and amplitudes of residual Ca^{2+} during high- (100 Hz, black) or low-frequency (2 Hz, red) activation starting from a resting Ca^{2+} (Ca_{rest}) level of 50 nM. ***C,*** Fraction of Ca^{2+} unoccupied SVs in the RRP (V) of the release sensor during the initial three activations of a 100 Hz (black) or 2 Hz (red) activation train. Note that during the first three activations at low frequency the RRP relaxes to its initial (V=1, i.e. 100%) from a transient overfilling (V>1) prior to the next pulse while it continues to increase in size during high-frequency activation due to the build-up in residual Ca^{2+} and continuing recruitment of reluctant vesicles (cf. ***B***). ***D,*** Transmitter release rates during three activations at high (black) or low frequencies (red), normalized to the first release process. ***E,*** Paired pulse ratios (PPRs) calculated as the ratio of release probabilities in the i-th ($p_{r,i}$) and the first pulse ($p_{r,1}$) during 100 Hz (filled black) or 2 Hz (red) activations plotted against the logarithmically scaled stimulus number. Open circles show PPRs duringh100 Hz activations started in a previously depressed model. ***F,*** (left) One-pool model of Ca^{2+} binding and release according to Wölfel et al (2007) consisting of the "allosteric" sensor model (Lou et al., 2005) supplemented with a reloading step of 2 SVs/ms. In contrast to our experimental findings, this model generates low-frequency facilitation and high-frequency depression (right). ***G,*** (left) as in ***F*** but for two parallel, non-interacting pools of SVs differing in their release rate constants thereby generating a "fast releasing pool of SV" (release rate I_+ as in ***F***) and a "slowly releasing pool of SV" (release rate $J_+ < I_+$ as in ***F,*** Wölfel et al., 2007). Both models are restored via Ca^{2+} independent reloading steps of 2 SVs/ms. Note that similar to the model in ***F***, this simulation generates a high-frequency depression and a low-frequency facilitation.

Figure 7. Kinetics of recovery from LFD ***A,*** Left, superimposition of the time course of LFD and LFD$_{triplet}$ (triplet stimulation at 200 Hz) elicited successively in the

same cell after at least 10 successive stimuli at 0.033 Hz. Right, time course for recovery from depression probed 30 s after the end of both LFD and LFD$_{triplet}$ by a 0.033 Hz stimulation. For clarity, EPSC amplitudes were plotted against stimulus number for the left graph and against time for the right graph. The thick red and blue lines on the right graph represent the monoexponential fit of the recovery. Data could be fitted from the first EPSC recorded 30 s after the end of LFD, whereas the recovery after LFD$_{triplet}$, could only be satisfactorily fitted after 7 stimuli at 0.033 Hz. **B,** Superimposition of the EPSC peak amplitude mean values plotted against time and recorded during a 0.033 Hz stimulation protocol applied 30 s after LFD (red points, $n=8$) or after LFD$_{triplet}$ (triplet stimulation at 200 Hz, blue points, $n=6$). EPSC peak amplitudes were normalized to the mean value of EPSCs recorded during the plateau at 0.033 Hz. The thick red and blue lines on the right-hand graph represent the monoexponential fits. **C,** same values as in *B*, with the difference that the time axis was shifted by 90 sec for experimental values obtained during the recovery train applied after LFD$_{triplet}$ (blue points). **D,** Recovery from LFD$_{triplet}$ probed by 100 Hz train at the end of the LFD induction period, as indicated by the stimulation paradigm. Left, EPSC traces recorded during the 1st triplet stimulation at 2 Hz. Right, EPSC traces recorded during 100 Hz trains applied 500 ms, 10 s or 1 min. after LFD induction ended. Traces are superimposed with EPSCs recorded during a 100 Hz train applied in control conditions (gray traces). **E,** Superimposition of the first responses to the trains recorded in *D*. **F,** Mean values of EPSC amplitudes recorded during 100 Hz trains applied 500 ms, 10 s or 1 min. after the 2 Hz stimulation period ended.

Figure 8. The reluctant pool can be recruited by increasing p_r. **A,** Superimposition of the ESPC amplitude time courses, plotted against the stimulus number obtained in the same PC during LFD (left panels) and during the recovery from LFD (right panels) by

a 100 Hz train before and after an increase in $[Ca^{2+}]_e$ from 2.5 mM to 4 mM. The inset shows the same experiment with normalized EPSC amplitude. **B,** Mean value of EPSC amplitude during LFD (left panel) and during the recovery via a 100 Hz train (middle panel) in presence of 2.5 mM (same set of data than in Fig. 1*B*, 3*D*) and 4 mM $[Ca^{2+}]_e$. Numbers at the bottom of the graphs indicate the number of cells for each condition. Right panel, the values of the delay (MWRST, *p*=0.60), plateau of LFD (MWRST, *p*=0.69) and decay time (MWRST, *p*=0.87) were statistically identical in low (2.5 mM, gray bars) and high Ca^{2+} (4 mM, blue bars) conditions. Black and red bars correspond to median and mean values respectively **C,** Left panel, typical experiment showing the time course of EPSC amplitude before and after the application of 10 µM EGTA-AM. Black points correspond to EPSCs recorded during 0.033Hz stimulation, gray and red points during 2 Hz stimulations and purple points during the application of 10 µM EGTA-AM at 0.033 Hz. Right panel, superimposition of normalized ESPC amplitudes from the same experiment during LFD and during the recovery via a 100 Hz train. **D,** Left panel, values of EPSC amplitude before (gray points) and after (red points) application of EGTA-AM are statistically identical (paired t-test, *p*=0.61, *n*=9) at any stimulus number during LFD. At the opposite, early responses were slightly reduced after application of EGTA-AM during recovery by 100 Hz train (*p*=0.031 at stimulus #5 and stimulus #6, signed rank test, *n=6*) (right panel).